Discontinuity-Induced Bifurcation Cascades in Flows and Maps with Application to Models of the Yeast Cell Cycle

Mike R. Jeffrey[a], Harry Dankowicz[b,*]

[a] *Department of Engineering Mathematics, University of Bristol, England*
[b] *Department of Mechanical Science and Engineering, University of Illinois at Urbana-Champaign, USA*

Abstract

This paper applies methods of numerical continuation analysis to document characteristic bifurcation cascades of limit cycles in piecewise-smooth, hybrid-dynamical-system models of the eukaryotic cell cycle, and associated period-adding cascades in piecewise-defined maps with gaps. A general theory is formulated for the occurrence of such cascades, for example given the existence of a period-two orbit with one point on the system discontinuity and with appropriate constraints on the forward trajectory for nearby initial conditions. In this case, it is found that the bifurcation cascade for nearby parameter values exhibits a scaling relationship governed by the largest-in-magnitude Floquet multiplier, here required to be positive and real, in complete agreement with the characteristic scaling observed in the numerical study. A similar cascade is predicted and observed in the case of a saddle-node bifurcation of a period-two orbit, away from the discontinuity, provided that the associated center manifold is found to intersect the discontinuity transversally.

Keywords: grazing bifurcations, cell division, border collisions, saddle-node bifurcations, period-adding sequences
2010 MSC: 37C27, 37E05, 37G15

1. Introduction

Piecewise-defined maps are a subject of increasing scientific interest, particularly as a description of global dynamics in piecewise-smooth flows. A piecewise-defined map is defined smoothly only over the interior of a partition of its domain, with discontinuities and/or loss of differentiability on the boundaries of this partition. When a map is derived as a stroboscopic snapshot of a flow, discontinuities are often the result of tangential (*grazing*) contact between the flow and a hypersurface at which a discontinuity in the vector field or the instantaneous state is introduced. In the neighborhood of grazing contact, small perturbations cause the forward dynamics to either intersect the hypersurface, or miss it, creating a corresponding discontinuity in the global dynamics. Well-known examples of piecewise-defined maps pertaining to grazing arise in the mechanics of impact and fluid layer contact. Piecewise-defined maps have been studied in their own right, for example in models of heart arrhythmia, neuron firing, and electrical power converters; see di Bernardo *et al.* [1] for a review.

The application focus of this paper is on hybrid dynamical models of the cell cycle of budding yeast (cf. Li *et al.* [2], Pfeuty and Kaneko [3], Tyson and Novák [4], and Qu *et al.* [5], but see also Noel *et al.* [6] and Alfieri *et al.* [7] for the construction of switched models of the cell cycle) designed to replicate experimentally observed processes of eukaryotic cell growth. In these models, the growth cycle exhibits exponential increase of cell mass, accompanied by variations in activator and inhibitor protein concentrations, modeled by a set of coupled nonlinear ordinary differential equations. When the concentration of a key protein falls below a critical value, the models considered here assume an essentially instantaneous cell division (mitosis) event, resulting in two progeny cells, each carrying a fraction of the mass of the mother cell. A period-p orbit represents a periodic sequence of p cycles of cell growth over which the mass at mitosis assumes p different values. In particular, period-one orbits result in regular cell cycles where the mass at mitosis is the same each time.

A *discontinuity-induced bifurcation* [1] occurs in a piecewise-smooth system, when the presence of a discontinuity results in a bifurcation that is unanticipated by the local description of the flow about some reference trajectory in the case that the discontinuity were to be ignored (without destroying the existence of the reference trajectory). In the cell-cycle models, an obvious example of a discontinuity-induced bifurcation is the disappearance (under further parameter variations) of a period-p orbit when the state during one of the cell cycles grazes the division threshold. A local analysis of return maps near such a grazing orbit yields a piecewise-defined map that is discontinuous across some hypersurface of initial conditions. In the piecewise-affine case, such a "map with a gap" (see Hogan *et al.* [8]) is known to exhibit complicated bifurcation scenarios, including period-adding cascades, period-incrementing cascades, and robust chaotic

*All correspondence should be sent to: danko@illinois.edu. This work is partially supported by NSF grant no. DMS-1016467.

attractors (e.g., Dutta *et al.* [9], Rajpathak *et al.* [10], but see also Glendinning [11] and Keener [12] for an analysis of routes to chaos in general piecewise-defined maps).

In the present paper, we derive a small set of sufficient conditions for the existence of period-adding bifurcation cascades accumulating on a grazing bifurcation of a period-two orbit in such piecewise-defined maps and verify the theoretical predictions using careful numerical analysis of suitably-constructed boundary-value problems for the cell cycle models. The theoretical analysis is found to accurately describe cascades observed in the numerical analysis of the corresponding hybrid dynamical system models, both qualitatively and quantitatively, including the prediction of a characteristics scaling relationship. Although this relationship results from the essentially one-dimensional nature of the bifurcation cascade sufficiently close to the accumulation point, the analysis is independent of model dimension and does not require the reduction to a piecewise-defined one-dimensional map.

We further derive a similar set of sufficient conditions for the existence of a period-adding bifurcation cascade accumulating on a saddle-node bifurcation of a period-two orbit, with no point of grazing contact with the system discontinuity. Remarkably, although the saddle-node bifurcation is not induced by the discontinuity, the associated bifurcation cascade is very much a result of the presence of the discontinuity. We here find a discontinuity-induced bifurcation scenario that is triggered by a saddle-node bifurcation, specifically, a saddle-node point on an infinite-period orbit that intersects the discontinuity transversally. We are not aware of any existing treatment or observation of such a global bifurcation scenario in a piecewise-smooth dynamical system.

A key ingredient of the conditions that hold at the accumulation point of the period-adding bifurcation cascades is the reinjection of a neighborhood of a grazing point on the discontinuity into the basin of attraction of the period-two orbit by the application of a state reset. This reinjection persists qualitatively even after the period-two orbit is destroyed by the discontinuity, but the asymptotic convergence to the locus of the period-two orbit (had the discontinuity been ignored) is interrupted by a crossing of the discontinuity and another global excursion away from the discontinuity. The scenario is reminiscent of examples of intermittency and bursting in the literature (cf. Dias De Deus *et al.* [13] and Mosekilde *et al.* [14]), but the dependence of the frequency of bursting on the parameter deviation from the accumulation point in the cascade may differ. A similar "homoclinic" behavior, with identical implications to the existence of a period-adding cascade may be found in Budd and Piiroinen [15].

In the remainder of this paper, we introduce and explore numerically two models of the yeast cell cycle in Sec. 2 and develop the corresponding theoretical treatment in Sec. 3. A concluding discussion in Sec. 5 reflects on the implications of the analysis to general piecewise-smooth dynamical systems and the class of cell cycle models considered herein. Several appendices at the end of the paper present examples of the phenomenology in the case of piecewise-affine, one-dimensional (complete treatment) and two-dimensional (numerical example) maps, piecewise-nonlinear one-dimensional maps (numerical example), and an autonomous linear oscillator with state resets (numerical example).

2. Cascades in models of the yeast cell cycle

2.1. Model formulation

We ground the theoretical analysis of this paper in the context of finite-dimensional, deterministic models of the cell cycle of budding yeast, and establish in these models several realizations of the abstract framework considered in the second half of the paper.

To this end, let u_i, for $i = 1, \ldots, 8$, represent nondimensionalized concentrations of eight key proteins that activate or inhibit different processes in the cycle of growth and division of eukaryotic cells, including the production or degradation of other members of this group of proteins. Specifically, following Tyson and Novák [4], let the continuous-time evolution of the cell state be governed by the following system of differential equations

$$\dot{u}_1 = k_1 - (k_2' + k_2'' u_2 + k_2''' u_4) u_1, \tag{1}$$

$$\dot{u}_2 = \frac{(k_3' + k_3'' u_4)(1 - u_2)}{J_3 + 1 - u_2} - \frac{(k_4 m u_b + k_4' u_7) u_2}{J_4 + u_2}, \tag{2}$$

$$\dot{u}_3 = k_5' + k_5'' \frac{(m u_b)^n}{J_5^n + (m u_b)^n} - k_6 u_3, \tag{3}$$

$$\dot{u}_4 = \frac{k_7 u_5 (u_3 - u_4)}{J_7 + u_3 - u_4} - \frac{k_8 M u_4}{J_8 + u_4} - k_6 u_4, \tag{4}$$

$$\dot{u}_5 = k_9 m u_b (1 - u_5) - k_{10} u_5, \tag{5}$$

$$\dot{u}_6 = k_{11} - (k_{12}' + k_{12}'' u_7 + k_{12}''' m u_b) u_6, \tag{6}$$

$$\dot{u}_7 = k_{13}' + k_{13}'' u_8 - k_{14} u_7, \tag{7}$$

$$\dot{u}_8 = \frac{(k_{15}' m + k_{15}'' u_7)(1 - u_8)}{J_{15} + 1 - u_8} - \frac{(k_{16}' + k_{16}'' m u_b) u_8}{J_{16} + u_8}, \tag{8}$$

where

$$u_b = u_1 - \frac{2 u_1 u_6}{\Sigma + \sqrt{\Sigma^2 - 4 u_1 u_6}} \tag{9}$$

and

$$\Sigma = u_1 + u_6 + \frac{1}{K_{eq}}, \tag{10}$$

and where the nondimensionalized cell mass is governed by the logistic growth model

$$\dot{m} = r m \left(1 - \frac{m}{\bar{m}}\right) \tag{11}$$

with carrying capacity $\bar{m}$. Moreover, suppose that a transversal intersection of the continuous-time trajectory with the zero-level surface of the scalar-valued function

$$h_{\text{mitosis}}(u) := u_1 - \bar{u}_1, \tag{12}$$

in the direction of decreasing values of h_{mitosis}, results in the instantaneous state reset

$$m \mapsto \rho m, \quad 0 < \rho < 1 \tag{13}$$

corresponding to a division of the mother cell into two daughter cells with masses ρm and $(1-\rho)m$, respectively. In the study below, we thus trace the time histories for the components of u and the cell mass m through generations of mother and daughter cells inheriting, at each division, the fraction ρ of the original cell mass.

There are 39 different parameters in the hybrid dynamical system governed by Eqs. (1-13), including the rate constants k_i, the Michaelis-Menten constants J_i, the division threshold $\bar{u}_1$, the growth rate r, and the carrying capacity $\bar{m}$. The majority of these will be fixed to values considered physically reasonable, given in [4] in a consistent set of units as: $k_1 = 0.04$, $k_2'' = 1$, $k_2''' = 1$, $k_3' = 1$, $k_3'' = 10$, $k_4 = 35$, $k_4' = 2$, $k_5' = 0.005$, $k_5'' = 0.2$, $k_6 = 0.1$, $k_7 = 1$, $k_8 = 0.5$, $k_9 = 0.1$, $k_{10} = 0.02$, $k_{11} = 1$, $k_{12}' = 0.2$, $k_{12}'' = 50$, $k_{12}''' = 100$, $k_{13}' = 0$, $k_{13}'' = 1$, $k_{14} = 1$, $k_{15}' = 1.5$, $k_{15}'' = 0.05$, $k_{16}' = 1$, $k_{16}'' = 3$, $J_3 = 0.04$, $J_4 = 0.04$, $J_5 = 0.3$, $J_7 = 10^{-3}$, $J_8 = 10^{-3}$, $J_{15} = 0.01$, $J_{16} = 0.01$, $K_{eq} = 10^3$, $M = 1$, $\bar{m} = 10$, $\bar{u}_1 = 0.1$, $n = 4$, $\rho = 0.5$. We will allow k_2' to vary, observing phenomena over a range from 0.04, the value given in [4], to around 0.2. We also take a value of $r = 0.0165$ that differs slightly from the values 0.01 and 0.005 that appear in [4].

Time histories of interest in this system tend to take the form of a succession of long and short intervals of growth, with longer intervals characterized by an additional local minimum in u_1 followed by an additional local maximum prior to cell division. As an example, Fig. 1 shows the projection of an example periodic steady-state behavior of the nine-dimensional dynamical system for $k_2' = 0.1524$, obtained using forward integration. Here, two distinct cell cycles (from the so-called *G1 phase* immediately following cell division and back) constitute a full period of the system behavior. In both of these cycles, a protein concentration modeled by u_1 initially decreases from the critical threshold $\bar{u}_1$ and then rises above this threshold to a local maximum. In the shorter of the two cell cycles, u_1 then decays monotonically in time until cell division is triggered. The duration[1] of this first cycle is $T_{\text{short}} = 35.0914$. In the longer of the two cell cycles, the monotonic decay of u_1 that previously led to cell division is here interrupted by a local minimum of u_1, a phase of increasing values of u_1, followed by another phase of monotonic decay and subsequent cell division. The duration of this second cycle is $T_{\text{long}} = 66.3226$.

The two crucial events that occur along a cycle, particularly (as we will see) for identifying bifurcations, are local minima of u_1 that occur for $u_1 > \bar{u}_1$, and the cell division events that occur at $u_1 = \bar{u}_1$. To this end, we consider

[1]The system of units implicit in the choice of parameter values measures time in minutes

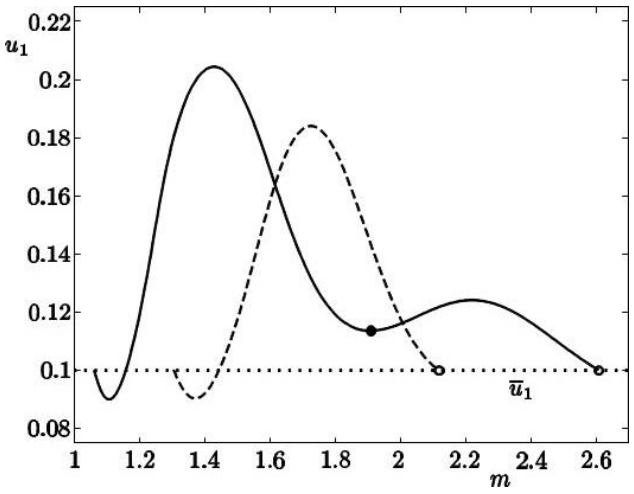

Figure 1: An example two-cycle, asymptotically stable periodic trajectory of the nine-dimensional hybrid dynamical system in Sec. 2.1 obtained for $k_2' = 0.1524$. Here and in Fig. 3, the filled circle indicates the local minimum in the value of u_1 above the critical level $\bar{u}_1$ at the terminal end of the first segment, whereas the open circles indicate terminal points on $\{h_{\text{mitosis}} = 0\}$, corresponding to the triggering of cell division. The solid curve represents the longer cell cycle of duration $T_{\text{long}} \approx 66$ min, while the dashed curve represents the shorter cell cycle of duration $T_{\text{short}} \approx 35$ min.

a maximal partition of system trajectories into individual segments that terminate either at a local minimum of u_1, i.e., on the zero-level surface of

$$h_{\text{minimum}}(u) := k_1 - (k_2' + k_2'' u_2 + k_2''' u_4)\, u_1, \tag{14}$$

with $h_{\text{mitosis}}(u) > 0$, or on $\{h_{\text{mitosis}} = 0\}$. In the former case, continuity in time implies the imposition of the identity

$$g_{\text{turn}} := (u, m) \mapsto (u, m)\,, \tag{15}$$

whereas termination on the zero-level surface of h_{mitosis} implies the imposition of the map

$$g_{\text{divide}} := (u, m) \mapsto (u, \rho m) \tag{16}$$

corresponding to a discrete jump in state space to a different point on this zero-level surface. The two-cycle, periodic, steady-state behavior may now be obtained as the solution to a three-segment, sequential boundary-value problem, in which each segment must satisfy the governing differential equations on its interior, and for which boundary conditions are given by the vanishing of the corresponding *event function* h_{minimum} or h_{mitosis} at the terminal point, and by the connectivity with the next segment expressed in terms of the corresponding *jump function* g_{turn} or g_{divide}.

A solution to the three-segment boundary-value problem is a *viable physical solution*, provided that state resets occur only at points on $\{h_{\text{mitosis}} = 0\}$ with h_{mitosis} locally decreasing. Suppose, for example, that all terminal points on $\{h_{\text{minimum}} = 0\}$ are local minima. In this case, a violation of viability along a one-parameter family of solutions occurs if the value of h_{mitosis} at the

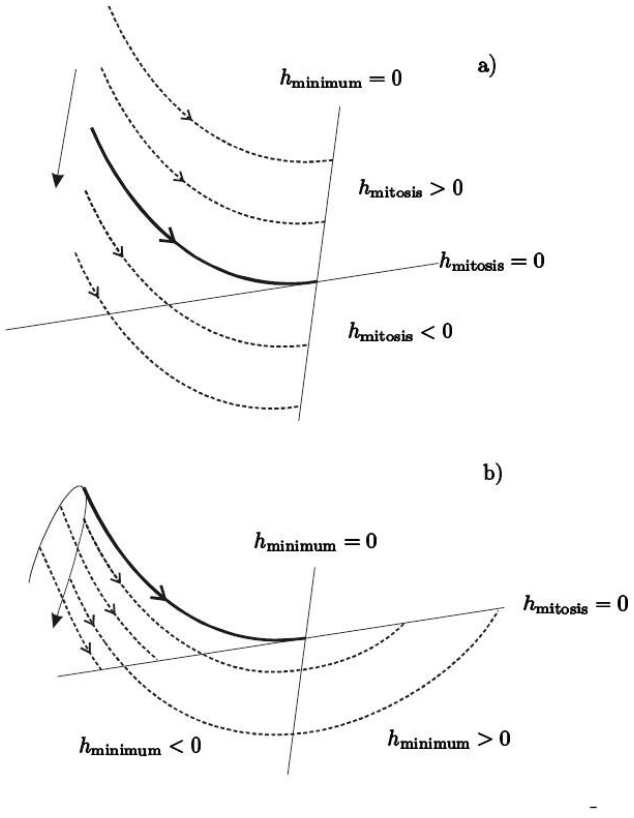

Figure 2: a) A Type I grazing bifurcation in which the value of h_{mitosis} at terminal points on $\{h_{\text{minimum}} = 0\}$ decreases through 0 under a parameter variation represented by the straight arrow. b) A Type II grazing bifurcation in which the value of h_{minimum} at terminal points on $\{h_{\text{mitosis}} = 0\}$ increases through 0 under a parameter variation represented by the curved arrow. In both cases, the grazing trajectory is represented by the thicker curve. Dashed curves represent actual solutions to the multisegment boundary-value problem.

terminal point on $\{h_{\text{minimum}} = 0\}$ changes from positive to negative, since h_{mitosis} is stationary and not decreasing on $\{h_{\text{minimum}} = 0\}$. At the special point where the value of h_{mitosis} vanishes at the terminal point on $\{h_{\text{minimum}} = 0\}$, the continuous-time trajectory is locally tangential to $\{h_{\text{mitosis}} = 0\}$ at a point of *grazing contact*. We refer to a parameter choice for which such a grazing contact occurs as corresponding to a *Type I grazing bifurcation* (cf. panel a) of Fig. 2).

Alternatively, a violation of viability along a one-parameter family of solutions occurs if the value of h_{minimum} at one of the terminal points on $\{h_{\text{mitosis}} = 0\}$ changes from negative to positive. At the special point where the value of h_{minimum} vanishes at a terminal point on $\{h_{\text{mitosis}} = 0\}$, the continuous-time trajectory is again locally tangential to the zero-level surface of h_{mitosis} at a point of grazing contact. We refer to a parameter choice for which such a grazing contact occurs as corresponding to a *Type II grazing bifurcation* (cf. panel b) of Fig. 2)..

It is clear from the nontrivial action of the state reset map g_{divide} that either of the two types of grazing bifurcations are associated with terminal points along branches of viable physical solutions to the three-segment boundary-value problem. In the case of a Type I grazing bifurcation, the approach to the grazing bifurcation parameter value is not reflected in any of the local properties of the corresponding state-space trajectory, with well-defined limits for the solutions of the associated variational equations. In the terminology of Dankowicz and Schilder [16], the tangent vector to a one-parameter family of solutions through such a grazing bifurcation has a nonzero component in the direction of an active continuation parameter.

In contrast, in the case of a Type II grazing bifurcation, the analysis in Dankowicz and Katzenbach [17] demonstrates a local behavior best described with the inclusion of a term dependent on the square-root of h_{minimum} at the terminal point. In this case, unbounded growth of one of the Floquet multipliers is observed as one approaches the grazing bifurcation parameter value. Moreover, the component in the direction of the active continuation parameter of the tangent vector to a one-parameter family of solutions through such a grazing bifurcation must equal zero at the bifurcation point, corresponding to a geometric fold of the solution branch.

Finally, a violation in spirit, albeit not immediately of the physical constraints of the problem, occurs when the terminal point on $\{h_{\text{minimum}} = 0\}$ is a point of tangential contact with this surface, corresponding to the merger of a local minimum and a local maximum at a saddle. A one-parameter family of solutions through such a point generically exhibits a geometric fold at the critical point, such that the terminal point on $\{h_{\text{minimum}} = 0\}$ switches from being a local minimum to a local maximum, as the solution manifold retraces the same overall state-space trajectory in the opposite direction of changes to the active continuation parameter.

In the analysis below, we restrict attention to multisegment solutions of the governing differential equations, together with the state reset, that satisfy the viability conditions described above. In particular, we observe the accumulation of sequences of Type I and Type II grazing bifurcations of periodic orbits of successively higher period onto limit points given by Type I grazing bifurcations and saddle-node bifurcations of two-cycle periodic orbits, such as that shown in Fig. 1.

2.2. Discretization

Generic forward-time trajectories of the hybrid dynamical system described in the previous section may be maximally partitioned into segments, in such a way that, except possibly for the last segment, terminal points lie either on $\{h_{\text{minimum}} = 0\}$ with $h_{\text{mitosis}} > 0$ or on $\{h_{\text{mitosis}} = 0\}$ with $h_{\text{minimum}} < 0$. For each such segment, we may characterize the terminal point (u_e, m_e) as the image of the corresponding initial point (u_b, m_b) under a map π_{mitosis} in the case that the terminating surface equals $\{h_{\text{mitosis}} = 0\}$ and π_{minimum} in the case that the terminating surface equals $\{h_{\text{minimum}} = 0\}$. With the possible exception of

the last segment, a maximally partitioned trajectory may then be described in terms of a composition of the maps $g_{\text{turn}} \circ \pi_{\text{minimum}}$ and $g_{\text{divide}} \circ \pi_{\text{mitosis}}$, referred to as its *signature*. As an example, the three-segment, two-cycle periodic orbit may be equivalently described in terms of a solution to the following system of equations

$$(u_{b,2}, m_{b,2}) = (g_{\text{turn}} \circ \pi_{\text{minimum}})\,(u_{b,1}, m_{b,1}) \tag{17}$$

$$(u_{b,3}, m_{b,3}) = (g_{\text{divide}} \circ \pi_{\text{mitosis}})\,(u_{b,2}, m_{b,2}) \tag{18}$$

$$(u_{b,1}, m_{b,1}) = (g_{\text{divide}} \circ \pi_{\text{mitosis}})\,(u_{b,3}, m_{b,3}) \tag{19}$$

or, equivalently, in terms of a fixed point of the map $\phi_{\text{short}} \circ \phi_{\text{long}}$, where the maps

$$\phi_{\text{short}} := g_{\text{divide}} \circ \pi_{\text{mitosis}} \tag{20}$$

and

$$\phi_{\text{long}} := g_{\text{divide}} \circ \pi_{\text{mitosis}} \circ g_{\text{turn}} \circ \pi_{\text{minimum}} \tag{21}$$

correspond to the short and long cell cycles described above.

As long as all terminal points correspond to points of transversality of the vector field with the corresponding event surfaces, a signature defines a nonsingular multisegment boundary-value problem with a *dimensional deficit* equal to the number of system parameters plus the state-space dimension. As discussed above, families of solutions to such a boundary-value problem may include subfamilies that violate the viability conditions, associated with Type I or Type II grazing bifurcations or the loss of transversality at a terminal point on $\{h_{\text{minimum}} = 0\}$.

We obtain a systematic numerical procedure for analyzing a multisegment boundary-value problem, such as that described above, by approximating the solution on each segment with a continuous, piecewise-polynomial function of time, expressed on each of N equal-sized[2] intervals in terms of its values at $m+1$ maximally distributed points on the interval. Finally, we require that the approximating polynomial satisfy the governing differential equations at m *collocation nodes* within each interval (here obtained from the roots of the m-th order Legendre polynomial). If we let n represent the state-space dimension (here equal to 9), for each segment we thus obtain $Nmn+(N-1)n$ equations in the $N(m+1)n+1$ unknowns given by the nodal values of the state vector and the duration of the segment. A closed system of nonlinear algebraic equations results from the imposition of $n+1$ additional conditions on each segment or, alternatively, a total of $k(n+1)$ conditions on the totality of unknowns for a trajectory consisting of k segments.

As an example, consider the imposition of a given set of initial conditions $\begin{pmatrix} u_0 & m_0 \end{pmatrix}^T$ on a solution segment. When a continuous, piecewise-polynomial function of time exists that satisfies the initial conditions, the collocation conditions, and the terminating condition at a point of transversality, the intersection with the zero-level surface of the corresponding event function is generically locally unique and persistent under changes in the initial conditions. As before, we associate this intersection with the image of the initial condition under the (implicitly defined) map π_{mitosis} in the case that the terminating surface equals $\{h_{\text{mitosis}} = 0\}$ and π_{minimum} in the case that it equals $\{h_{\text{minimum}} = 0\}$, albeit recognizing that these maps are at best approximations of the maps defined for the infinite-dimensional problem.

An approximation of the three-segment, two-cycle periodic orbit found above may now be equivalently described in terms of a solution to the discretized version of the boundary-value problem in Eqns. (17-19) or, equivalently, in terms of a fixed point of the composition $\phi_{\text{short}} \circ \phi_{\text{long}}$ of the discretized maps ϕ_{short} and ϕ_{long}, again corresponding to the short and long cell cycles described above.

The one-dimensional family of periodic, three-segment solution trajectories in Fig. 3a) shows the result of applying the `hspo` toolbox (compatible with the continuation package referred to below as COCO [16]) to numerical continuation of solutions to the corresponding discretized boundary-value problem with $N = 40$ and $m = 4$ under variations in k_2'. The interval of existence is here bounded i) from below by a Type I grazing bifurcation at $k_2' = k_{2,\text{grazing}}' := 0.11606$, where the second segment terminates at a point on $\{h_{\text{minimum}} = 0\} \cap \{h_{\text{mitosis}} = 0\}$; and ii) from above by a geometric fold at $k_2' = k_{2,\text{fold}}' := 0.19810$, where the local minimum in u_1 merges with the subsequent local maximum at a saddle point. The corresponding periodic orbits are shown in Figs. 3b) and c), respectively.

Continuation of the periodic, three-segment solution trajectory through the fold at $k_2' = k_{2,\text{fold}}'$ is possible, but simply retraces the previous solution branch in the opposite direction, with the first solution segment terminating on the local maximum, rather than the local minimum. Instead, continuation of the actual periodic system behavior beyond $k_{2,\text{fold}}'$ requires a resegmentation of the solution into a two-segment trajectory consisting only of segments terminating on $\{h_{\text{mitosis}} = 0\}$.

Of greater physical (biological) relevance, however, is the local behavior of the system for k_2' below $k_{2,\text{grazing}}'$. At the grazing bifurcation point, the three-segment periodic trajectory is locally asymptotically stable in the Lyapunov sense (provided that we ignore the possible imposition of g_{divide} on the vicinity of the terminal point of the first solution segment). The largest-in-magnitude eigenvalue of the Jacobian of the composition $\phi_{\text{short}} \circ \phi_{\text{long}}$ is here

[2] We comment on nonuniform, adaptive partitions and questions pertaining to numerical accuracy in Sec. 5.

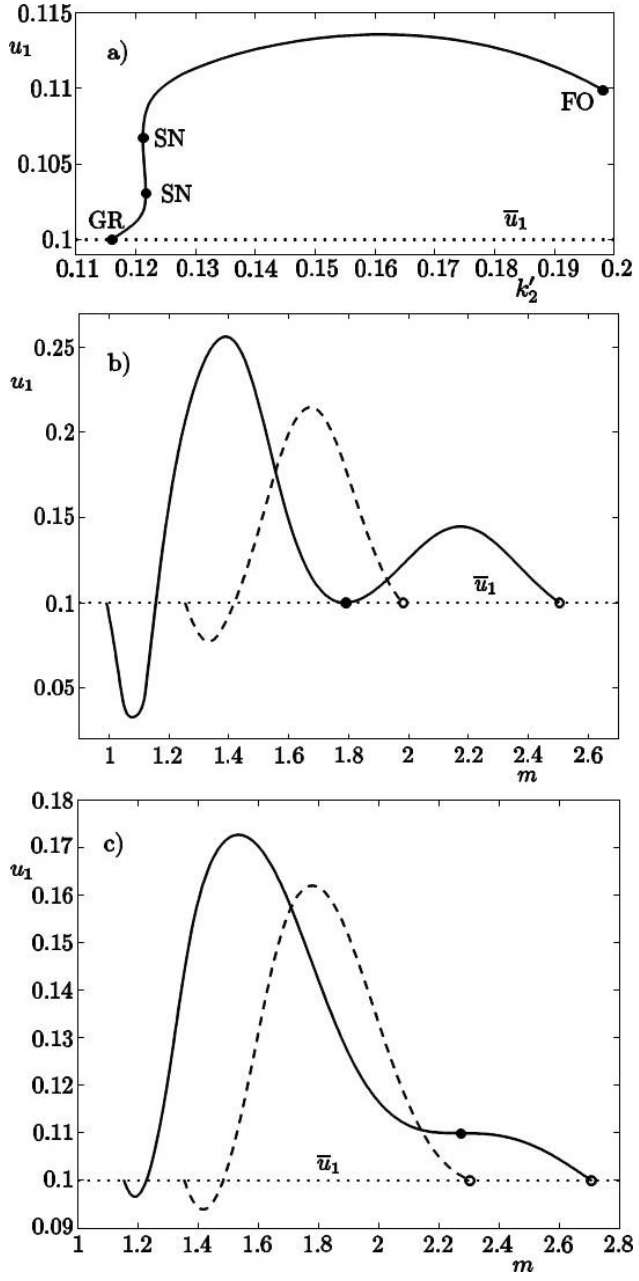

Figure 3: a) A one-dimensional branch of viable, three-segment solution trajectories obtained with COCO under variations in k_2'. Here, each point on the solution manifold is represented by the value of h_{mitosis} at the terminal point of the first solution segment. The two saddle-node bifurcations (denoted by SN) correspond to a single eigenvalue of the Jacobian of the composition $\phi_{\text{short}} \circ \phi_{\text{long}}$ evaluated at the fixed point crossing the unit circle at 1. The terminal points of the solution branch are coincident with a Type I grazing bifurcation (denoted by GR) and a geometric fold (denoted by FO) associated with the merger of the local minimum at the terminal point of the first segment with a subsequent local maximum along the second segment. The corresponding solution trajectories are shown in panels b) and c), respectively. Here, solid curves represent long cell cycles and dashed curves represent short cell cycles.

$\lambda_{\max} = 0.4332$ with corresponding eigenvector given by

$$v_{\max} = \begin{pmatrix} 0.0000 \\ -0.0001 \\ -0.8207 \\ -0.1736 \\ -0.0706 \\ 0.0023 \\ -0.0056 \\ -0.0066 \\ -0.5397 \end{pmatrix} \tag{22}$$

For small perturbations of the initial condition on the first solution segment away from that of the grazing trajectory, two possible scenarios are found in the case of forward iterates of $g_{\text{divide}} \circ \pi_{\text{mitosis}}$ or $g_{\text{turn}} \circ \pi_{\text{minimum}}$, as appropriate, (this time accounting for the possible imposition of g_{divide} on the vicinity of the terminal point of the first solution segment of the grazing trajectory). In the first case, the solution trajectory is patterned upon the grazing periodic trajectory for the entire length of the transient, i.e., corresponding to alternating application of ϕ_{long} and ϕ_{short}, such that the sequence of terminal points on $\{h_{\text{mitosis}} = 0\}$ at the end of a short cell cycle converges monotonically to the corresponding terminal point on the grazing trajectory along $v_{\max}$ with a local rate of convergence approximately given by $\lambda_{\max}$. In the second case, illustrated in Fig. 4, the initial perturbation results first in the application of ϕ_{short} before again following an alternating sequence of long and short cycles, resulting in an eventually monotonically convergent sequence of terminal points on $\{h_{\text{mitosis}} = 0\}$ along $v_{\max}$, at the end of the short cell cycle, with a local rate of convergence given by $\lambda_{\max}$.

2.3. A period-adding sequence

For small and positive integer values of n, forward integration beyond initial transients may be used to establish the existence of windows of periodic orbits corresponding to fixed points of the composition $(\phi_{\text{short}} \circ \phi_{\text{long}})^n \circ \phi_{\text{short}}$ for values of k_2' close to, but below $k_{2,\text{grazing}}'$. Several examples are shown in Fig. 5a). In each case, parameter continuation of the corresponding multisegment boundary-value problem using `hspo` with $N = 40$ and $m = 4$, and with k_2' as active continuation parameter, yields a one-dimensional solution manifold that terminates at the more distal end from $k_{2,\text{grazing}}'$ at a Type I grazing bifurcation, and at the more proximal end from $k_{2,\text{grazing}}'$ at a Type II grazing bifurcation (cf. panels b) and c) of Fig. 5). As predicted by the theory above, the corresponding Floquet multipliers approach finite limits at the Type I grazing bifurcations, but exhibit unbounded growth at the Type II grazing bifurcations. For $n = 1, \ldots, 4$, the periodic orbits are all asymptotically stable near the Type I grazing bifurcations. A geometric fold is found in the vicinity of the Type II grazing bifurcation for $n = 1$ as one real Floquet multiplier passes through 1 on its way to positive infinity at a discontinuity-induced saddle-node bifurcation. For $n = 2$,

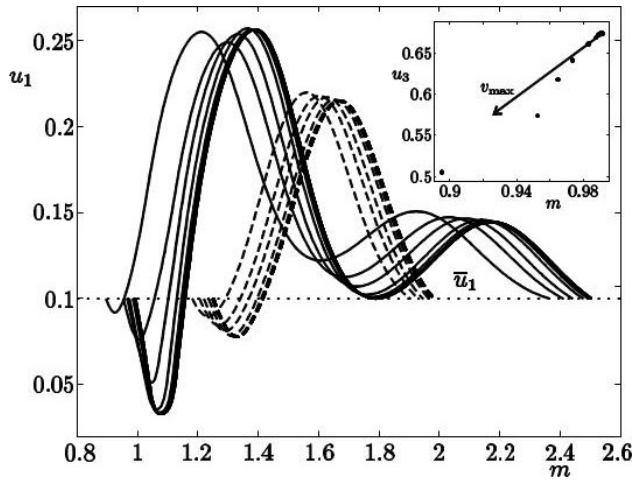

Figure 4: Forward trajectory obtained by applying ϕ_{long} and ϕ_{short} alternately, and as implied by the viability conditions, to the initial condition generated by applying ϕ_{short} (rather than ϕ_{long}) to the fixed point of $\phi_{\text{short}} \circ \phi_{\text{long}}$ corresponding to the period-two orbit at the Type I grazing bifurcation point. The inset shows the sequence of images of ϕ_{short} along this trajectory, and the convergence to the fixed point along $v_{\max}$ with a local rate of convergence given by $\lambda_{\max}$. Here, solid curves represent long cell cycles and dashed curves represent short cell cycles.

3, and 4, the Type II grazing bifurcation is associated with a discontinuity-induced period-doubling bifurcation as one real Floquet multiplier passes through -1 on its way to negative infinity.

As supported by panels c) and b), respectively, of Fig. 5, we observe that the Type II grazing bifurcations always correspond to a grazing of the first trajectory segment, whereas the Type I grazing bifurcations correspond to grazing of the last trajectory segment that terminates on $\{h_{\text{minimum}} = 0\}$ in the application of the composition $(\phi_{\text{short}} \circ \phi_{\text{long}})^n \circ \phi_{\text{short}}$ to the corresponding fixed point. We may locate such grazing bifurcation parameter values by imposing a condition on the values of h_{minimum} and h_{mitosis}, respectively, at the corresponding terminal points, and solving the new multisegment boundary-value problem for the value of k_2'. Moreover, for some sufficiently large integer n^*, our analysis shows that an initial solution guess for a multisegment periodic trajectory corresponding to some $n > n^*$ may be obtained by $n - n^*$ repetitions of the last pair of long and short cell cycles in the multisegment trajectory obtained for n^*. The grazing bifurcation parameter values shown in Table 1 were obtained using this methodology.

Let $k'_{2,n,+}$ and $k'_{2,n,-}$ denote the parameter values for the Type I and Type II grazing bifurcations, respectively, of the periodic orbit corresponding to the fixed point of the map $(\phi_{\text{short}} \circ \phi_{\text{long}})^n \circ \phi_{\text{short}}$. As seen in the third and fourth columns of Table 1, the ratios

$$r_{n,\pm} := \frac{k'_{2,n+2,\pm} - k'_{2,n+1,\pm}}{k'_{2,n+1,\pm} - k'_{2,n,\pm}} \tag{23}$$

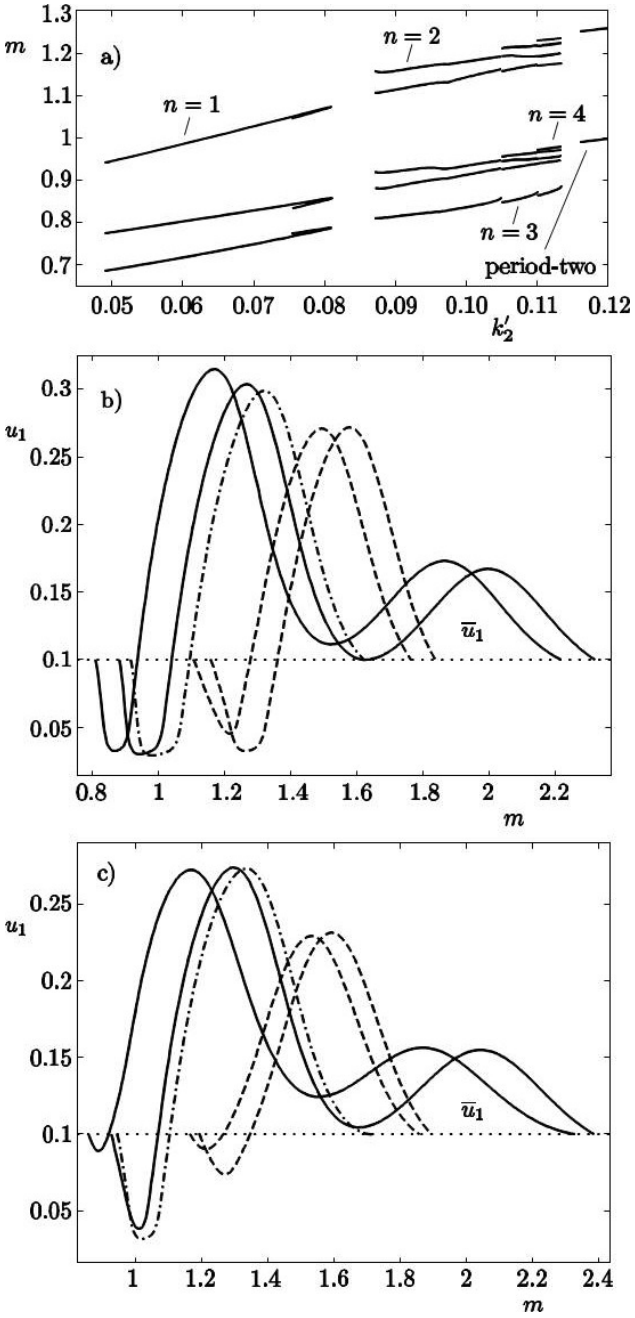

Figure 5: a) Branches of periodic orbits corresponding to fixed points of the composition $(\phi_{\text{short}} \circ \phi_{\text{long}})^n \circ \phi_{\text{short}}$ for $n = 1$, 2, 3, and 4 as well as the two-cycle orbit discussed in Sec. 2.2, under variations in k_2'. Each point corresponds to the value of m at the beginning of a cell cycle. The terminal points of the solution branches obtained for $k_2' < k'_{2,\text{grazing}}$ are coincident with Type I grazing bifurcations (distal from $k'_{2,\text{grazing}}$) and Type II grazing bifurcations (proximal from $k'_{2,\text{grazing}}$). The corresponding solution trajectories for $n = 2$ are shown in panels b) and c), respectively. Here, solid curves represent long cell cycles and dashed curves represent short cell cycles. The dash-dotted curve represents the initial short cell cycle.

Table 1: Sequences of Type I and Type II grazing bifurcation parameter values and the corresponding ratios between successive differences of bifurcation parameter values near $k'_{2,\text{grazing}}$.

n	$k'_{2,n,+}$	$k'_{2,n,-}$	$r_{n,+}$	$r_{n,-}$
1	0.049015	0.075416	0.4644	0.1721
2	0.087191	0.104879	0.2847	0.6610
3	0.104923	0.109949	0.6584	0.4210
4	0.109971	0.113299	0.4244	0.4913
5	0.113295	0.114710	0.4927	0.5101
6	0.114706	0.115403	0.5108	0.4742
7	0.115401	0.115757	0.4740	0.4519
8	0.115756	0.115925	0.4515	0.4415
9	0.115924	0.116000	0.4412	0.4368
10	0.116000	0.116034	0.4366	0.4348
11	0.116034	0.116048	0.4346	0.4339
12	0.116048	0.116055	0.4337	0.4335
13	0.116055	0.116058	0.4334	0.4333
14	0.116058	0.116059	0.4332	0.4332

between successive differences of bifurcation parameter values appear to converge to a number very close to the eigenvalue $\lambda_{\max}$. Indeed, consider the sequence $k'^{*}_{2,n}$, such that each of the ratios

$$\frac{k'_{2,n+1,\pm} - k'^{*}_{2,n}}{k'_{2,n,\pm} - k'^{*}_{2,n}} \tag{24}$$

between successive deviations from $k'^{*}_{2,n}$ of the grazing bifurcation parameter values equals $\lambda_{\max}$. In this case, we find that, as n grows, $k'^{*}_{2,n}$ converges to $k'_{2,\text{grazing}}$ to within $8 * 10^{-12}$ when $n = 18$.

2.4. A global bifurcation

As an alternative to the 9-dimensional model of the cell cycle dynamics considered above, we restrict attention in this section to a simplified 4-dimensional model (also given in [4], whose continuous-time dynamics are governed by the system of differential equations

$$\dot{u}_1 = k_1 - k'_2 u_1 - k''_2 u_1 u_2, \tag{25}$$

$$\dot{u}_2 = \frac{(k'_3 + k''_3 u_3)(1 - u_2)}{J_3 + 1 - u_2} - \frac{k_4 m u_1 u_2}{J_4 + u_2}, \tag{26}$$

$$\dot{u}_3 = k'_5 + k''_5 \frac{(m u_1)^n}{J_5^n + (m u_1)^n} - k_6 u_3 \tag{27}$$

and

$$\dot{m} = r m \left(1 - \frac{m}{\bar{m}}\right), \tag{28}$$

and where a transversal intersection of the continuous-time trajectory with the zero-level surface of the scalar-valued function

$$h_{\text{mitosis}}(u) := u_1 - \bar{u}_1, \tag{29}$$

in the direction of decreasing values of h_{mitosis}, again results in the instantaneous state reset

$$m \mapsto \rho m, \quad 0 < \rho < 1. \tag{30}$$

We retain identical values for the model parameters as in the previous section, except that here $r = 0.01$ and k'_2 is allowed to vary over a considerably larger range.

With the identical methodology to that described in the previous section, we again find an asymptotically stable, two-cycle, periodic orbit of the four-dimensional dynamical system for $k'_2 = 0.155$. Numerical continuation with k'_2 as active continuation parameter of the corresponding three-segment discretized boundary-value problem yields the one-parameter solution manifold shown in Fig. 6a). A novel element is the geometric fold at $k'_2 = k'_{2,\text{fold}} := 0.15396$ corresponding to a saddle-node bifurcation where a single real Floquet multiplier leaves the unit circle in the complex plane through 1. The solution branch terminates at a Type I grazing bifurcation at $k'_2 = 0.15430$ and at a Type II grazing bifurcation at $k'_2 = 0.17133$, preceded by a discontinuity-induced period-doubling bifurcation.

When $k'_2 = k'_{2,\text{fold}}$, two possible scenarios are found in the case of forward iterates of $g_{\text{divide}} \circ \pi_{\text{mitosis}}$ or $g_{\text{turn}} \circ \pi_{\text{minimum}}$, as appropriate, applied to initial perturbations from the fixed point of $\phi_{\text{short}} \circ \phi_{\text{long}}$ along the eigenvector v_{fold} corresponding to the single eigenvalue 1 on the unit circle. In the first case, the solution trajectory is patterned upon the two-cycle periodic orbit for the entire length of the transient, i.e., corresponding to alternating application of ϕ_{long} and ϕ_{short}, such that the sequence of terminal points on $\{h_{\text{mitosis}} = 0\}$ at the end of a long cell cycle converges monotonically to the corresponding terminal point on the nonhyperbolic periodic trajectory along v_{fold} with a local rate of convergence that approaches 1. In the second case, the initial perturbation results in the application of a finite number of iterates of $\phi_{\text{short}} \circ \phi_{\text{long}}$ followed by one additional iterate of ϕ_{short} before again following an alternating sequence of long and short cycles, and an eventually monotonically convergent sequence of terminal points on $\{h_{\text{mitosis}} = 0\}$, at the end of each short cycle, approaching the nonhyperbolic fixed point along the eigenvector v_{fold} (cf. Fig. 7).

Remarkably, for small and positive integer values of n, numerical experiments again yield a sequence of windows of periodic orbits corresponding to fixed points of the composition $(\phi_{\text{short}} \circ \phi_{\text{long}})^n \circ \phi_{\text{short}}$ for values of k'_2 close to, but below $k'_{2,\text{fold}}$. Several examples are shown in Fig. 8a). In each case, parameter continuation of the corresponding multisegment boundary-value problem using `hspo` and with k'_2 as active continuation parameter yields a one-dimensional solution manifold that terminates at the more distal end from $k'_{2,\text{fold}}$ at a Type I grazing bifurcation and at the more proximal end from $k'_{2,\text{fold}}$ at a Type II grazing bifurcation (cf. panels b) and c) in Fig. 8). As before, the corresponding Floquet multipliers approach finite limits at the Type I grazing bifurcations, but exhibit unbounded growth at the Type II grazing bifurcations. For $n = 2$ and 3, the periodic orbits are asymptotically stable near the Type I grazing bifurcations. Discontinuity-induced period-doubling bifurcations are found in the vicinity of the Type II grazing bifurcations as one real Floquet multiplier passes

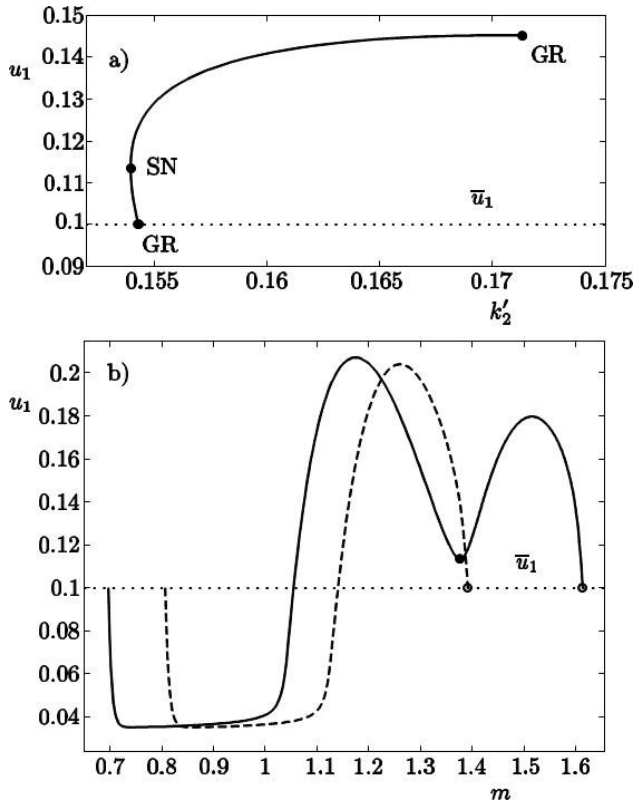

Figure 6: a) A one-dimensional branch of viable, three-segment solution trajectories obtained with COCO under variations in k_2' for the hybrid dynamical system in Sec. 2.4. Here, each point on the solution manifold is represented by the value of h_{mitosis} at the terminal point of the first solution segment. The saddle-node bifurcation (denoted by SN) correspond to a single eigenvalue of the Jacobian of the composition $\phi_{\text{short}} \circ \phi_{\text{long}}$ evaluated at the fixed point crossing the unit circle at 1. The terminal points of the solution branch are coincident with a Type I and a Type II grazing bifurcation, respectively (both denoted by GR). The nonhyperbolic solution trajectory is shown in panel b). Here, solid curves represent long cell cycles and dashed curves represent short cell cycles. The filled circle indicates the local minimum in the value of u_1 above the critical level $\bar{u}_1$ at the terminal end of the first segment, whereas the open circles indicate terminal points on $\{h_{\text{mitosis}} = 0\}$, corresponding to the triggering of cell division.

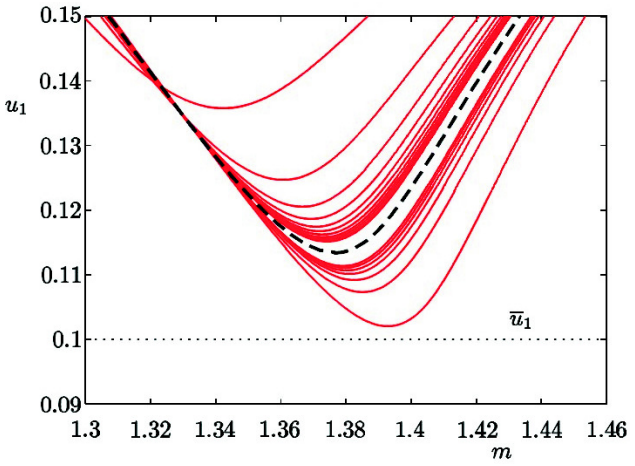

Figure 7: Forward trajectory obtained by applying ϕ_{long} and ϕ_{short} alternately, and as implied by the viability conditions, to the initial condition generated by applying a small perturbation along v_{fold} to the fixed point of $\phi_{\text{short}} \circ \phi_{\text{long}}$ corresponding to the period-two orbit at the saddle-node bifurcation point, here represented by the dashed curve. The figure shows trajectory segments near the local minimum in u_1 above $\bar{u}_1$ during each long cell cycle. Minima located below the dashed curve successively approach the critical level of u_1. The lowest curve belongs to a long cell cycle that is followed by two consecutive short cell cycles and a return to a long cell cycle along the topmost curve in the figure.

through -1 on its way to negative infinity.

We again obtain numerical values for the Type I and Type II grazing bifurcation parameter values by relying on the `hspo` toolbox for multisegment periodic orbits corresponding to fixed points of $(\phi_{\text{short}} \circ \phi_{\text{long}})^n \circ \phi_{\text{short}}$ with the corresponding grazing condition on the last trajectory segment that terminates on $\{h_{\text{minimum}} = 0\}$, or on the first trajectory segment, respectively. The grazing bifurcation parameter values shown in Table 2 were obtained using this methodology.

Let $k'_{2,n,+}$ and $k'_{2,n,-}$ again denote the parameter values for the Type I and Type II grazing bifurcations, respectively, of the periodic orbit corresponding to the fixed point of the map $(\phi_{\text{short}} \circ \phi_{\text{long}})^n \circ \phi_{\text{short}}$. As seen from the third and fourth columns of Table 2, the sequences of differences

$$d_{n,\pm} := \frac{1}{\sqrt{k'_{2,n+1,\pm} - k'_{2,\text{fold}}}} - \frac{1}{\sqrt{k'_{2,n,\pm} - k'_{2,\text{fold}}}} \tag{31}$$

appear to approach a finite limit as n grows, consistent with the observation that

$$k'_{2,n+1,\pm} - k'_{2,\text{fold}} \sim n^{-2} \tag{32}$$

for large n.

A further notable distinction between the bifurcation cascade observed here and in the previous section is illustrated in Figs. 5a) and 8a). In the case of cascade associated with the Type I grazing bifurcation of an asymptotically stable, two-cycle, periodic orbit, an accumulation of trajectory segments along the higher-period orbits is found in the vicinity of the grazing periodic orbit, and thus in the vicinity of the discontinuity that separates locally between the application of ϕ_{short} and ϕ_{long}. In contrast, in the case of the cascade associated with the saddle-node bifurcation of the two-cycle, periodic orbit, an accumulation of trajectory segments along the higher-period orbits is found in the vicinity of the nonhyperbolic periodic orbit, and thus **not** in the vicinity of the discontinuity that separates locally between application of ϕ_{short} and ϕ_{long}.

3. A piecewise-defined map

We proceed to develop an abstract model of the dynamics of the hybrid dynamical systems considered in the pre-

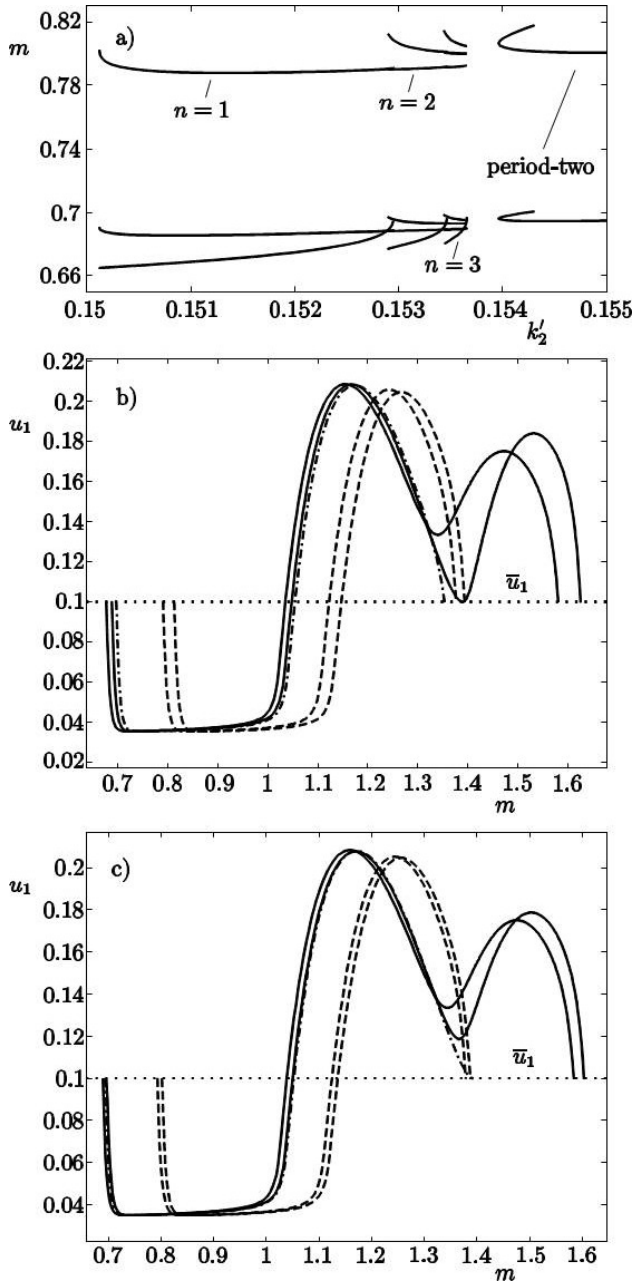

Figure 8: a) Branches of periodic orbits corresponding to fixed points of the composition $(\phi_{\text{short}} \circ \phi_{\text{long}})^n \circ \phi_{\text{short}}$ for $n = 1$, 2, and 3, as well as the two-cycle orbit discussed in Sec. 2.4, under variations in k_2'. Each point corresponds to the value of m at the beginning of a cell cycle. The terminal points of the solution branches are coincident with a Type I grazing bifurcations (distal from $k'_{2,\text{fold}}$ and Type II grazing bifurcations (proximal from $k'_{2,\text{fold}}$. The corresponding solution trajectories for $n = 2$ are shown in panels b) and c), respectively. Here, solid curves represent long cell cycles and dashed curves represent short cell cycles. The dash-dotted curve represents the initial short cell cycle.

Table 2: Sequences of Type I and Type II grazing bifurcation parameter values and successive differences between the corresponding reciprocal square roots of the deviations from $k'_{2,\text{fold}}$.

n	$k'_{2,n,+}$	$k'_{2,n,-}$	$d_{n,+}$	$d_{n,-}$
1	0.150127	0.152956	14.48	13.13
2	0.152896	0.153461	13.14	12.66
3	0.153440	0.153658	12.70	12.44
4	0.153649	0.153757	12.46	12.30
5	0.153752	0.153814	12.32	12.22
6	0.153811	0.153850	12.23	12.16
7	0.153848	0.153874	12.17	12.13
8	0.153873	0.153891	12.14	12.11
9	0.153890	0.153904	12.11	12.09
10	0.153903	0.153913	12.09	12.08
11	0.153913	0.153920	12.08	12.07
12	0.153920	0.153926	12.07	12.07
13	0.153926	0.153931	12.07	12.06
14	0.153931	0.153935	12.06	12.06

vious section, with the aim of establishing sufficient conditions for the occurrence of cascades of grazing bifurcations and period-adding sequences as observed in the numerical analysis in Sec. 2.

To this end, consider again the description of the forward-time dynamics for initial conditions on some neighborhood on $\{h_{\text{mitosis}} = 0\}$ of the fixed point (u^*, m^*) of the map $\phi_{\text{short}} \circ \phi_{\text{long}}$ for $k_2' = k'_{2,\text{grazing}}$. By transversality, it follows that there exists a locally smooth, codimension-one, embedded submanifold through this fixed point, characterized by the local properties that

1. trajectories based at points on this manifold reach $\{h_{\text{minimum}} = 0\}$ at points of grazing contact with $\{h_{\text{mitosis}} = 0\}$;
2. trajectories based at points on one side of the manifold reach $\{h_{\text{mitosis}} = 0\}$ before $\{h_{\text{minimum}} = 0\}$;
3. trajectories based at points on the other side of the manifold reach $\{h_{\text{minimum}} = 0\}$ before $\{h_{\text{mitosis}} = 0\}$.

In the first case, the subsequent forward-time dynamics are ambiguous and may be thought of as reflecting the limiting behavior for initial conditions in each of the two other cases. In particular, in the second case, the subsequent imposition of the state reset g_{divide} yields a new initial condition on $\{h_{\text{mitosis}} = 0\}$ in the vicinity of $\phi_{\text{short}}(u^*, m^*)$. As described in the previous section, subsequent iterates of the return map to $\{h_{\text{mitosis}} = 0\}$, including the imposition of the state reset, are described by an alternating application of ϕ_{long} and ϕ_{short}. Indeed, after a sufficiently large number of iterates, the sequence of subsequent image points accumulates on (u^*, m^*).

In contrast, in the third case, the subsequent forward-time dynamics include the return to $\{h_{\text{mitosis}} = 0\}$ and imposition of the state reset g_{divide} to yield a new initial condition on $\{h_{\text{mitosis}} = 0\}$ in the vicinity of $\phi_{\text{long}}(u^*, m^*)$. As

the forward-time dynamics based at $\phi_{\text{long}}(u^*, m^*)$ are unambiguously described by the application of π_{mitosis}, it follows that the subsequent dynamics in the third case, after a second imposition of g_{divide}, yield a new initial condition on $\{h_{\text{mitosis}} = 0\}$ in the vicinity of $(\phi_{\text{short}} \circ \phi_{\text{long}})(u^*, m^*) = (u^*, m^*)$.

It is important to recognize that the description of the forward-time dynamics in terms of the maps ϕ_{short} and ϕ_{long} does not generalize to initial conditions outside of the local neighborhood of (u^*, m^*). Indeed, such initial conditions may be associated with signatures of a different form than could be obtained by compositions of ϕ_{short} and ϕ_{long}. For the purposes of the required abstraction, however, we are only concerned with forward-time dynamics based near (u^*, m^*), for which the maps ϕ_{short} and ϕ_{long} suffice.

Finally, we observe that although the embedded submanifold, corresponding to trajectory segments that reach $\{h_{\text{mitosis}} = 0\}$ at points of grazing contact, depends on k_2', a smooth local coordinate transformation will render this dependence of sufficiently high-order in the deviation from $k'_{2,\text{grazing}}$ so as to be negligible in the subsequent analysis.

Inspired by these observations, we proceed to restrict attention to a piecewise-defined map

$$\phi_\mu : x \mapsto \begin{cases} \phi_L(x, \mu) & \text{when } x \in \Omega_L \subset \mathbb{R}^n, \\ \phi_R(x, \mu) & \text{when } x \in \Omega_R \subset \mathbb{R}^n, \end{cases} \tag{33}$$

for $\mu \in \mathbb{R}$ on some neighborhood of 0. In particular, let $B_r(0)$ denote the ball of radius r centered on the origin. We then assume that, for δ sufficiently small,

$$\Omega_L \cap B_\delta(0) = \{h \leq 0\} \cap B_\delta(0) \tag{34}$$

and

$$\Omega_R \cap B_\delta(0) = \{h \geq 0\} \cap B_\delta(0) \tag{35}$$

for some smooth function $h : \mathbb{R}^n \to \mathbb{R}$ such that $h(0) = 0$ and $\partial_x h(0) \neq 0$. Here, ϕ_L and ϕ_R correspond directly to ϕ_{long} and ϕ_{short}, whereas h must be operationally defined from the forward dynamics of the differential equations in Sec. 2, as suggested above. We let μ represent a characteristic bifurcation parameter, e.g., corresponding to $k'_{2,\text{grazing}} - k'_2$ in the case of the cell-cycle dynamics in Sec. 2.3.

3.1. A border-collision bifurcation

Let

$$\Phi_{L,\mu}(x) := \phi_R(\phi_L(x, \mu), \mu) \tag{36}$$

and suppose that

$$\Phi_{L,0}(0) = 0, \tag{37}$$

where $\phi_L(0, 0) \in \Omega_R$. It follows that $x = 0$ is a period-two point of the piecewise-smooth map ϕ_0 and a zero of the function

$$F(x, \mu) := x - \Phi_{L,\mu}(x) \tag{38}$$

for $\mu = 0$. Let

$$J_L := \partial_x \phi_L(0, 0) \tag{39}$$

and

$$J_R := \partial_x \phi_R(\phi_L(0, 0), 0). \tag{40}$$

A persistent family $x_L^*(\mu)$ of such zeros under variations in μ then follows by the implicit-function theorem, provided that

$$\partial_x F(0, 0) = I - J_R \cdot J_L \tag{41}$$

is invertible. In this case, let

$$\kappa_L := \partial_\mu \phi_L(0, 0) \tag{42}$$

and

$$\kappa_R := \partial_\mu \phi_R(\phi_L(0, 0), 0). \tag{43}$$

By implicit differentiation of $F(x_L^*(\mu), \mu) \equiv 0$ with respect to μ and evaluation at $\mu = 0$, it follows that

$$\partial_\mu x_L^*(0) = (I - J_R \cdot J_L)^{-1} \cdot (\kappa_R + J_R \cdot \kappa_L). \tag{44}$$

Provided that

$$\partial_x h(0) \cdot (I - J_R \cdot J_L)^{-1} \cdot (\kappa_R + J_R \cdot \kappa_L) > 0, \tag{45}$$

and for sufficiently small but negative μ, each member of the family $x_L^*(\mu)$ thus corresponds to a period-two point of the piecewise-smooth map ϕ_μ. If, in addition, all eigenvalues of the Jacobian $J_R \cdot J_L$ have magnitude less than 1, the fixed point $x_L^*(\mu)$ of $\Phi_{L,\mu}$ is asymptotically stable in the Lyapunov sense and the corresponding period-two orbit is orbitally stable with zero asymptotic phase for all sufficiently small perturbations.

We proceed to assume that $\phi_R(0, 0) \neq \phi_L(0, 0)$. It follows that $\mu = 0$ is a terminal point on the branch of period-two orbits described by $x_L^*(\mu)$ and that asymptotic stability in the sense of Lyapunov of $x_L^*(\mu)$ is lost at the corresponding *border collision bifurcation*. Now suppose that the largest-in-magnitude eigenvalue $\lambda_{\max}$ of the Jacobian $J_R \cdot J_L$ is real and positive, and that the corresponding eigenvector $v_{\max}$ is transversal to the zero-level surface of h. Finally, assume that $h \neq 0$ on all iterates of the forward trajectory under ϕ_0 of the initial condition $\phi_R(0, 0)$, and that there exists an integer N, such that the sequence $\left\{\phi_0^{N+2i}(\phi_R(0, 0))\right\}_{i=0}^{\infty}$ lies in Ω_L and converges (monotonically in h) to 0 with asymptote given by the eigenvector $v_{\max}$. In particular, for sufficiently large N,

$$\phi_0^{N+2i}(\phi_R(0, 0)) = \Phi_{L,0}^i\left(\phi_0^N\left(\phi_R(0, 0)\right)\right) \tag{46}$$

for all $i \geq 0$.

It now follows that there exists a δ, such that

$$h\left(\Phi_{L,0}^i\left(\phi_0^N\left(\phi_R(x, 0)\right)\right)\right) < 0 \tag{47}$$

for $i \geq 0$ and $x \in \{h = 0\} \cap B_\delta(0)$. Moreover, since $\partial_x h(0) \cdot \partial_\mu x_L^*(0) > 0$, it follows that for $0 < \mu^* \ll 1$, there exists an integer $M^+(\mu^*)$, such that

$$h\left(\Phi_{L,\mu^*}^i\left(\phi_{\mu^*}^N\left(\phi_R(x, \mu^*)\right)\right)\right) > 0 \tag{48}$$

for all $i \geq M^+(\mu^*)$. As μ varies from 0 to μ^*, the surface $\Phi_{L,\mu}^{M^+(\mu^*)}\left(\phi_\mu^N\left(\phi_R(x,\mu)\right)\right)$ extrudes a volume with one terminal face for $\mu = 0$ in $h < 0$, and the other terminal face for $\mu = \mu^*$ in $h > 0$ (cf. Fig. 11). Moreover, by the contractive nature of the composition $\Phi_{L,0}$ near 0, it follows that the intersection of this volume with the set of initial conditions $\{h = 0\} \cap B_\delta(0)$ must be contained strictly within the latter set, in such a way that the distance between any two points has been reduced relative to the original distance by some factor > 1. By the contraction mapping theorem, it follows that, for each sufficiently large integer n, there exists a μ_n^+ such that

$$\Phi_{L,\mu_n^+}^n\left(\phi_{\mu_n^+}^N\left(\phi_R(x,\mu_n^+)\right)\right) = x, \tag{49}$$

for some unique point x in $\{h = 0\} \cap B_\delta(0)$, i.e., that x is a fixed point of the map $\Phi_{L,\mu}^n\left(\phi_\mu^N\left(\phi_R(\cdot,\mu)\right)\right)$ for $\mu = \mu_n^+$. Since $\Phi_{L,0}(0) = 0$, we may rely on the identical argument to conclude the existence of a μ_n^-, for sufficiently large integers n, such that

$$\Phi_{L,\mu_n^-}^{n-1}\left(\phi_{\mu_n^-}^N\left(\phi_R(\Phi_{L,\mu_n^-}(x),\mu_n^-)\right)\right) = x \tag{50}$$

for some unique point x in $\{h = 0\} \cap B_\delta(0)$, for some $\delta > 0$, i.e., that $\Phi_{L,\mu}(x)$ is a fixed point of the map $\Phi_{L,\mu}^n\left(\phi_\mu^N\left(\phi_R(\cdot,\mu),\mu\right)\right)$ for $\mu = \mu_n^-$.

It follows from the above analysis (and the assumptions on κ_L, κ_R, J_L, and J_R) that, for sufficiently large n, the parameter values μ_n^+, μ_n^- are associated with terminal points along a family of periodic trajectories of period $2n+N+1$, corresponding to border-collision bifurcations with the discontinuity at $\{h = 0\}$. In the limit of large n, the fixed points lie arbitrarily close to the origin and the iterated dynamics $\Phi_{L,\mu}$ in the vicinity of 0 may be described in terms of a one-dimensional map with Jacobian $\lambda_{\max}$ whose iterates represent projections of the deviation from the origin onto $v_{\max}$. It follows that the bifurcation points accumulate monotonically on $\mu = 0$ with a limiting scaling given by $\lambda_{\max}$.

We relate the border-collision bifurcation points to the grazing bifurcation points in Sec. 2.3 by recognizing that a fixed point of $\Phi_{L,\mu}^n\left(\phi_\mu^N\left(\phi_R(\cdot,\mu),\mu\right)\right)$ on $\{h = 0\}$ corresponds to a Type II grazing bifurcation, whereas a fixed point of $\Phi_{L,\mu_n^-}^{n-1}\left(\phi_{\mu_n^-}^N\left(\phi_R(\Phi_{L,\mu_n^-}(\cdot),\mu_n^-)\right)\right)$ on $\{h = 0\}$ corresponds to a Type I grazing bifurcation. The near-grazing dependence on the square-root of h associated with a Type II grazing bifurcation must here be reflected in a locally nonlinearizable form of the map ϕ_R at $x = 0$ (cf. Dutta and Banerjee [18] and Pring and Budd [19]). For sufficiently large n, the periodic orbits must therefore be highly unstable. In contrast, when ϕ_R is linearizable at $x = 0$ (as illustrated by the example one-dimensional, piecewise-affine map with a gap in 4.1), for sufficiently large n, the periodic orbits are all asymptotically stable on their intervals of existence.

3.2. A saddle-node bifurcation

In lieu of the assumptions made in the previous section, suppose that for $\mu < 0$ and sufficiently small, there exists a pair of families of fixed points $x_L^*(\mu)$ and $x_L^{**}(\mu)$ of $\Phi_{L,\mu}$, such that $\phi_L\left(x_L^*(\mu),\mu\right), \phi_L\left(x_L^{**}(\mu),\mu\right) \in \Omega_R$ and such that the two families merge when $\mu = 0$ at a saddle-node bifurcation where a single eigenvalue crosses the unit circle through 1, while all other eigenvalues remain within the unit circle.

Denote by v_{fold} the eigenvector corresponding to the eigenvalue 1 of the Jacobian of $\Phi_{L,0}$ evaluated at the degenerate fixed point. Suppose that the part of the center manifold, for which forward iterates of $\Phi_{L,\mu}$ move away from the fixed point, intersects the zero-level surface $\{h = 0\}$ for the first time (in arclength from the degenerate fixed point) at the origin, where $\phi_L(0,0) \neq \phi_R(0,0)$ and $\phi_L(0,0) \in \Omega_R$. Finally, suppose that $h \neq 0$ on all iterates of the forward trajectory under ϕ_0 of the initial condition $\phi_R(0,0)$, and that there exists an integer N such that the sequence $\left\{\phi_0^{N+2i}\left(\phi_R(0,0)\right)\right\}_{i=0}^\infty$ lies in Ω_L and converges monotonically to $x_L^*(0)$ with asymptote given by the eigenvector v_{fold}. For sufficiently large N, it again follows that

$$\phi_0^{N+2i}\left(\phi_R(0,0)\right) = \Phi_{L,0}^i\left(\phi_0^N\left(\phi_R(0,0)\right)\right) \tag{51}$$

for all $i \geq 0$.

The argument that led us to conclude the existence of the sequence μ_n^+ in the case of the grazing bifurcation of the two-cycle periodic orbit carries over essentially verbatim to the present case, with the difference that (following [13] and Duarte *et al.* [20], but see also 4.2), $\mu_n^+ \sim n^{-2}$ for sufficiently large n. With $\mu = k'_{2,\text{fold}} - k'_2$, the border collision bifurcation sequence corresponds to the sequence of Type I grazing bifurcations of the corresponding periodic trajectories in Sec. 2.4.

Since we no longer assume that $\phi_R(\phi_L(0,0),0) = 0$, the existence of a sequence μ_n^- must be obtained from an identical argument, but with the added and independent assumption that $h \neq 0$ on all iterates of the forward trajectory under ϕ_0 of the initial condition $\phi_R\left(\phi_L(0,0),0\right)$, and that there exists an integer $\tilde{N}$ such that the sequence $\left\{\phi_0^{\tilde{N}+2i}\left(\phi_R(\phi_L(0,0),0)\right)\right\}_{i=0}^\infty$ lies in Ω_L and converges monotonically to $x_L^*(0)$ with asymptote given by the eigenvector v_{fold}. With $\mu = k'_{2,\text{fold}} - k'_2$, the corresponding border collision bifurcation sequence consists of Type II grazing bifurcations of the corresponding periodic trajectories in Sec. 2.4.

Notably, in the case that either of the two forward trajectories under ϕ_0 considered above fail to satisfy the required criteria, then no conclusion may be drawn about the existence or nature of the corresponding sequence of border-collision bifurcation points. In contrast, in the case of a border-collision of the period-two orbit, the existence of one of these sequences of bifurcation points implies the existence of the other. In the saddle-node case, even if the required criteria are satisfied, the orbital signature (the

sequence of symbols L and R associated with the application of ϕ_L and ϕ_R, respectively) may differ between the two families of periodic orbits. In this case, the parameter values μ_n^+ and μ_n^- no longer correspond to terminal points along the same solution manifold.

4. Additional examples

4.1. Piecewise affine maps with gap

For purposes of illustrating the general theory for the case of a grazing period-two orbit, as obtained in Sec. 3.1, we focus in this section on example piecewise-affine maps with a finite discontinuity.

A one-dimensional map. Let

$$\phi_L : x \mapsto \lambda + \kappa_L \mu + v_L x, \tag{52}$$

and

$$\phi_R : x \mapsto -\lambda v_R + \kappa_R \mu + v_R x \tag{53}$$

where $\lambda > 0$, $v := v_R v_L \in (0,1)$, and without loss of generality

$$\kappa_L^* := \frac{\kappa_R + v_R \kappa_L}{1 - v} > 0. \tag{54}$$

In particular, when $\mu = 0$, it follows that $\phi_L(0) > 0$ and $\phi_R(\phi_L(0)) = 0$.

Now consider the one-dimensional piecewise affine map

$$x_{i+1} = \begin{cases} \phi_L(x_i) & \text{when } x_i \le 0, \\ \phi_R(x_i) & \text{when } x_i \ge 0. \end{cases} \tag{55}$$

We refer to the difference $\phi_L(0) - \phi_R(0) = \lambda(1+v_R)$ as the *discontinuity gap*. Notably, and in contrast to many previous studies, we do not identify a unique choice of ϕ_R or ϕ_L to be applied at the discontinuity. In the discussion that follows, it proves useful to consider each of these choices as giving the limiting behavior of the composite map as x tends to 0 from above and below, respectively, since arbitrarily close to, but away from this limit, the image of the map remains well-defined.

It is convenient to define the compositions $\Phi_L = \phi_R \circ \phi_L$ and $\Phi_R = \phi_L \circ \phi_R$. It follows, for example, that $\phi_R \circ \Phi_R^i = \Phi_L^i \circ \phi_R$ for every integer i. Straightforward algebra then shows the existence of a family of fixed points of Φ_L given by the formula

$$x_L^*(\mu) = \kappa_L^* \mu \tag{56}$$

or, equivalently, a family of fixed points of Φ_R given by the formula

$$x_R^*(\mu) = \phi_L(x_L^*(\mu)) = \lambda + \kappa_R^* \mu, \tag{57}$$

where

$$\kappa_R^* := \frac{\kappa_L + v_L \kappa_R}{1 - v}. \tag{58}$$

Together, the points $x_L^*(\mu)$ and $x_R^*(\mu)$ constitute a period-two orbit of the original dynamical system, if and only if

$$x_L^*(\mu) \le 0 \le x_R^*(\mu), \tag{59}$$

i.e., for sufficiently small, nonpositive μ. Under variations in μ, the case of $\mu = 0$ corresponds to a so-called *border-collision bifurcation*, as the branch of period-two orbits terminates at this parameter value with x_L^* on the discontinuity.

For $\mu < 0$, the period-two orbit found above is locally asymptotically stable, since $\partial_x \Phi_L$ and $\partial_x \Phi_R$ evaluated at $x_L^*(\mu)$ and $x_R^*(\mu)$, respectively, both equal v. For $\mu = 0$, however, the period-two orbit is, ast best, only locally asymptotically stable in the Lyapunov sense for the original dynamical system for one-sided perturbations.

The case of positive slope. Suppose that $v_R, v_L > 0$ and consider first the case when $\mu = 0$. Then, for initial conditions $x_0 \lesssim 0$,

$$x_{2i} = \Phi_L^i(x_0) = v^i x_0 \uparrow 0 = \Phi_L^i(0) \tag{60}$$

as $i \to \infty$. In contrast, for initial conditions $x_0 \gtrsim 0$,

$$x_{2i} = \Phi_R^i(x_0) = \lambda + v^i(x_0 - \lambda) \tag{61}$$

which converges from below to

$$\lambda = \Phi_R^i(\phi_L(0)) \tag{62}$$

as $i \to \infty$. In the limit as $x_0 \downarrow 0$, we conclude that

$$\Phi_R^i(0) \uparrow \Phi_R^i(\phi_L(0)) \tag{63}$$

and thus

$$\left(\phi_R \circ \Phi_R^i\right)(0) \uparrow \left(\phi_R \circ \Phi_R^i\right)(\phi_L(0)) \tag{64}$$

or, since

$$\phi_R \circ \Phi_R^i \circ \phi_L = \Phi_L^i \circ \phi_R \circ \phi_L = \Phi_L^{i+1}, \tag{65}$$

that

$$\left(\Phi_L^i \circ \phi_R\right)(0) = \left(\phi_R \circ \Phi_R^i\right)(0) \uparrow \Phi_L^{i+1}(0) = 0. \tag{66}$$

A cobweb representation of the corresponding trajectory is shown in Fig. 9.

Claim 1. *For arbitrary μ, fixed points of the map $\phi_R \circ \Phi_R^n$ for any integer n are given by*

$$x_{R,n}^{**}(\mu) = -\frac{v_R v^n}{1 - v_R v^n}\lambda + \frac{\kappa_L^* - \kappa_R^* v_R v^n}{1 - v_R v^n}\mu. \tag{67}$$

In particular,

$$\left(\phi_R \circ \Phi_R^{n-1}\right)\left(x_{R,n}^{**}(\mu)\right) = -\frac{v_R v^{n-1}}{1 - v_R v^n}\lambda + \left(\kappa_L^* + \frac{v_R v^{n-1}}{1 - v_R v^n}(\kappa_L^* - \kappa_R^*)\right)\mu. \tag{68}$$

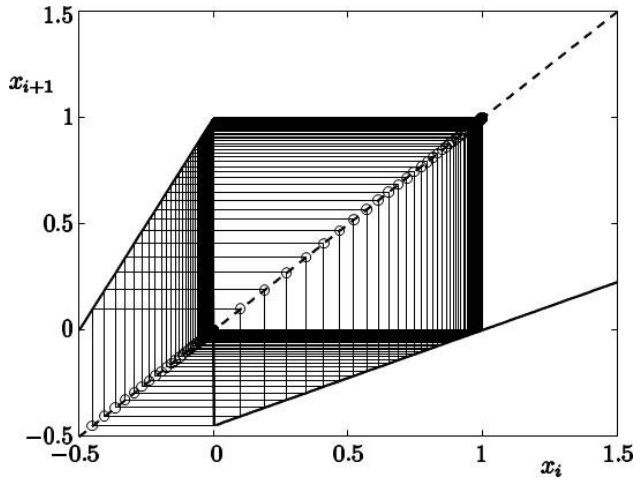

Figure 9: A cobweb representation of the forward trajectory of $\phi_R(0)$ for $\mu = 0$ in the case of $v_L = 2$ and $v_R = 0.45$. The asymptotic convergence to the period-two limit cycle satisfies the criteria in Sec. 3.1.

Proof. It follows by induction that

$$\Phi_R^k\left(x_{R,n}^{**}(\mu)\right) = \left(1 - \frac{v^k}{1 - v_R v^n}\right)\lambda + \left(\kappa_R^* + \frac{v^k}{1 - v_R v^n}\left(\kappa_L^* - \kappa_R^*\right)\right)\mu \quad (69)$$

and

$$\left(\phi_R \circ \Phi_R^k\right)\left(x_{R,n}^{**}(\mu)\right) = -\frac{v_R v^k}{1 - v_R v^n}\lambda + \left(\kappa_L^* + \frac{v_R v^k}{1 - v_R v^n}\left(\kappa_L^* - \kappa_R^*\right)\right)\mu. \quad (70)$$

and the claims follow from the substitutions $k \mapsto n$ and $k \mapsto n-1$, respectively, in Eq. (70). □

The fixed points $x_{R,n}^{**}(\mu)$ are periodic points of the original dynamical system iff

$$\Phi_R^k\left(x_{R,n}^{**}(\mu)\right) \geq 0 \quad (71)$$

for all $0 \leq k \leq n$ and

$$\left(\phi_R \circ \Phi_R^k\right)\left(x_{R,n}^{**}(\mu)\right) \leq 0 \quad (72)$$

for all $0 \leq k \leq n-1$.

Claim 2. *There exists a lower bound N, such that for each $n > N$, $x_{R,n}^{**}(\mu)$ is a periodic point of the original dynamical system iff $\mu \in [\mu_n^+, \mu_n^-] \subset \mathbb{R}_+$, where*

$$\mu_n^- := \frac{v_R v^n}{v\kappa_L^*\left(1 - v_R v^n\right) + v_R v^n\left(\kappa_L^* - \kappa_R^*\right)}\lambda \quad (73)$$

and

$$\mu_n^+ := \frac{v_R v^n}{\kappa_L^* - \kappa_R^* v_R v^n}\lambda. \quad (74)$$

Proof. It is straightforward to show that $[\mu_n^+, \mu_n^-] \subset \mathbb{R}_+$ for sufficiently large n. It follows from Eq. (67) that $x_{R,n}^{**} \geq 0$ for sufficiently large n if and only if $\mu \geq \mu_n^+$, since equality holds when $\mu = \mu_n^+$ and the slope of $x_{R,n}^{**}$ with respect to μ is positive for large n. Similarly, for $1 \leq k \leq n$, it follows from Eq. (69) that $\Phi_R^k\left(x_{R,n}^{**}\right) > 0$ for sufficiently large n and $\mu \in [\mu_n^+, \mu_n^-]$, since $\Phi_R^k\left(x_{R,n}^{**}\right)$ is linear in μ and positive at $\mu = \mu_n^+$ and $\mu = \mu_n^-$ for large n. Furthermore, it follows from Eq. (68) that $\left(\phi_R \circ \Phi_R^{n-1}\right)\left(x_{R,n}^{**}\right) \leq 0$ for sufficiently large n if and only if $\mu \leq \mu_n^-$, since equality holds when $\mu = \mu_n^-$ and the slope of $\left(\phi_R \circ \Phi_R^{n-1}\right)\left(x_{R,n}^{**}\right)$ with respect to μ is positive for large n. Finally, for $0 \leq k \leq n-2$, it follows from Eq. (70) that $\left(\phi_R \circ \Phi_R^k\right)\left(x_{R,n}^{**}\right) < 0$ for sufficiently large n and $\mu \in [\mu_n^+, \mu_n^-]$, since $\left(\phi_R \circ \Phi_R^k\right)\left(x_{R,n}^{**}\right)$ is linear in μ and negative at $\mu = \mu_n^+$ and $\mu = \mu_n^-$ for large n. □

Since

$$\frac{\mu_{n+1}^-}{\mu_n^+} = \frac{\kappa_L^* - \kappa_R^* v_R v^n}{\kappa_L^* - \kappa_R^* v_R v^n + \kappa_L^* v_R v^n (1 - v)} < 1, \quad (75)$$

it follows that the intervals of existence of each such periodic orbit are mutually disjoint. From Eqs. (73-74), it follows that $\mu_n^-, \mu_n^+ \downarrow 0$ as $n \to \infty$. Substitution now yields the limiting scaling relationships

$$\lim_{n\to\infty} \frac{\mu_{n+1}^+}{\mu_n^+} = \lim_{n\to\infty} \frac{\mu_{n+2}^+ - \mu_{n+1}^+}{\mu_{n+1}^+ - \mu_n^+} = v \quad (76)$$

and

$$\lim_{n\to\infty} \frac{\mu_{n+1}^-}{\mu_n^-} = \lim_{n\to\infty} \frac{\mu_{n+2}^- - \mu_{n+1}^-}{\mu_{n+1}^- - \mu_n^-} = v. \quad (77)$$

Given the same lower bound N on n, the local asymptotic stability of each of these periodic orbits on their respective interval of existence follows immediately from the linearity of the component maps. As evidenced by the proof of Claim 2, each interval is bounded by two border-collision bifurcations, corresponding either to $x_{R,n}^{**} = 0$ (when $\mu = \mu_n^+$) or $\left(\phi_R \circ \Phi_R^{n-1}\right)\left(x_{R,n}^{**}\right) = 0$ (when $\mu = \mu_n^-$). We thus observe an infinite sequence of border-collision bifurcations accumulating monotonically from the right on $\mu = 0$. Moreover, at $\mu = 0$, a border collision of a period-two orbit coexists with an infinite family of trajectories based arbitrarily close to $x = 0$ and whose odd iterates approach $x = 0$ arbitrarily closely in forward time.

The case of negative slope. Suppose that $v_R, v_L < 0$ and consider again the case when $\mu = 0$. Then, for initial conditions $x_0 \lesssim 0$, it again holds

$$x_{2i} = \Phi_L^i\left(x_0\right) = v^i x_0 \uparrow 0 = \Phi_L^i\left(0\right) \quad (78)$$

as $i \to \infty$. In contrast, for initial conditions $x_0 \gtrsim 0$,

$$x_i = \phi_R^i\left(x_0\right) = v_R^i x_0 - \frac{1 - v_R^i}{1 - v_R} v_R \lambda \quad (79)$$

when[3] $v_R > -1$ and

$$\begin{aligned} x_{2i+1} &= \left(\Phi_R^i \circ \phi_R\right)(x_0) \\ &= v^i v_R x_0 + \left(1 - v^i\left(1 + v_R\right)\right)\lambda \end{aligned} \tag{80}$$

when $v_R < -1$. In the former case, the forward trajectory clearly converges to the unique fixed point of ϕ_R at $x = -v_R\lambda/\left(1 - v_R\right)$, independently of x_0, thus violating the assumption on the forward trajectory of $\phi_R(0,0)$ required by the analysis in Sec. 3.1. In the case that $v_R < -1$, however, the odd iterates converge from above to

$$\lambda = \Phi_R^i\left(\phi_L\left(0\right)\right) \tag{81}$$

as $i \to \infty$. In the limit as $x_0 \downarrow 0$, we conclude that

$$\left(\Phi_R^i \circ \phi_R\right)(0) \downarrow \Phi_R^i\left(\phi_L\left(0\right)\right) \tag{82}$$

and thus

$$\left(\phi_R \circ \Phi_R^i \circ \phi_R\right)(0) \uparrow \left(\phi_R \circ \Phi_R^i\right)\left(\phi_L\left(0\right)\right) \tag{83}$$

or, since

$$\phi_R \circ \Phi_R^i \circ \phi_L = \Phi_L^i \circ \phi_R \circ \phi_L = \Phi_L^{i+1}, \tag{84}$$

that

$$\begin{aligned} \left(\Phi_L^i \circ \phi_R \circ \phi_R\right)(0) &= \left(\phi_R \circ \Phi_R^i \circ \phi_R\right)(0) \\ &\uparrow \Phi_L^{i+1}(0) = 0. \end{aligned} \tag{85}$$

A cobweb representation of the corresponding trajectory is shown in Fig. 10.

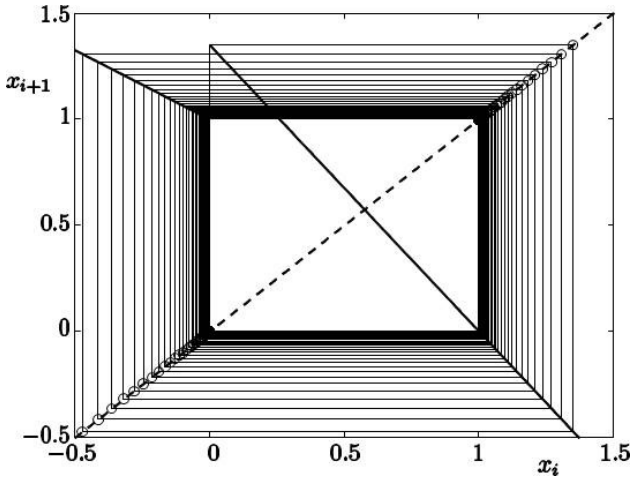

Figure 10: A cobweb representation of the forward trajectory of $\phi_R(0)$ for $\mu = 0$ in the case of $v_L = -0.65$ and $v_R = -1.35$. The asymptotic convergence to the period-two limit cycle again satisfies the criteria in Sec. 3.1.

[3]The case when $v_R = -1$ follows by taking the corresponding limit in Eq. (79).

Claim 3. *For arbitrary μ, fixed points of the composition $\phi_R \circ \Phi_R^n \circ \phi_R$ for any integer n are given by*

$$\begin{aligned} x_{R,n}^{**}(\mu) = &-\frac{v_R\left(1 + v_R\right)v^n}{1 - v_R^2 v^n}\lambda \\ &+ \left(\kappa_L^* + \frac{v_R\left(1 + v_R\right)v^n}{1 - v_R^2 v^n}\left(\kappa_L^* - \kappa_R^*\right)\right)\mu. \end{aligned} \tag{86}$$

In particular,

$$\begin{aligned} \left(\phi_R \circ \Phi_R^{n-1} \circ \phi_R\right)\left(x_{R,n}^{**}(\mu)\right) = &-\frac{v_R\left(1 + v_R\right)v^{n-1}}{1 - v_R^2 v^n}\lambda \\ &+ \left(\kappa_L^* + \frac{v_R\left(1 + v_R\right)v^{n-1}}{1 - v_R^2 v^n}\left(\kappa_L^* - \kappa_R^*\right)\right)\mu. \end{aligned} \tag{87}$$

Proof. It follows by induction that

$$\begin{aligned} \left(\Phi_R^k \circ \phi_R\right)\left(x_{R,n}^{**}(\mu)\right) = &\left(1 - \frac{\left(1 + v_R\right)v^k}{1 - v_R^2 v^n}\right)\lambda \\ &+ \left(\kappa_R^* + \frac{\left(1 + v_R\right)v^k}{1 - v_R^2 v^n}\left(\kappa_L^* - \kappa_R^*\right)\right)\mu \end{aligned} \tag{88}$$

and

$$\begin{aligned} \left(\phi_R \circ \Phi_R^k \circ \phi_R\right)\left(x_{R,n}^{**}(\mu)\right) = &-\frac{v_R\left(1 + v_R\right)v^k}{1 - v_R^2 v^n}\lambda \\ &+ \left(\kappa_L^* + \frac{v_R\left(1 + v_R\right)v^k}{1 - v_R^2 v^n}\left(\kappa_L^* - \kappa_R^*\right)\right)\mu. \end{aligned} \tag{89}$$

and the claims follow from the substitutions $k \mapsto n$ and $k \mapsto n - 1$, respectively, in Eq. (89). □

The fixed points $x_{R,n}^{**}(\mu)$ are periodic points of the original dynamical system iff $x_{R,n}^{**}(\mu) \geq 0$,

$$\left(\Phi_R^k \circ \phi_R\right)\left(x_{R,n}^{**}(\mu)\right) \geq 0 \tag{90}$$

for all $0 \leq k \leq n$ and

$$\left(\phi_R \circ \Phi_R^k \circ \phi_R\right)\left(x_{R,n}^{**}(\mu)\right) \leq 0 \tag{91}$$

for all $0 \leq k \leq n - 1$.

Claim 4. *There exists a lower bound N, such that for each $n > N$, $x_{R,n}^{**}(\mu)$ is a periodic point of the original dynamical system iff $\mu \in [\mu_n^+, \mu_n^-] \subset \mathbb{R}_+$, where*

$$\mu_n^- := \frac{v_R\left(1 + v_R\right)v^n}{v\kappa_L^*\left(1 - v_R^2 v^n\right) + v_R\left(1 + v_R\right)v^n\left(\kappa_L^* - \kappa_R^*\right)}\lambda \tag{92}$$

and

$$\mu_n^+ := \frac{v_R\left(1 + v_R\right)v^n}{\kappa_L^* - \kappa_R^* v_R v^n + v_R v^n\left(\kappa_L^* - \kappa_R^*\right)}\lambda. \tag{93}$$

Proof. It is straightforward to show that $[\mu_n^+, \mu_n^-] \subset \mathbb{R}_+$ for sufficiently large n. It follows from Eq. (86) that $x_{R,n}^{**} \geq 0$ for sufficiently large n if and only if $\mu \geq \mu_n^+$, since equality holds when $\mu = \mu_n^+$ and the slope of $x_{R,n}^{**}$ with respect to μ is positive for large n. Similarly, for $0 \leq k \leq n$, it follows from Eq. (88) that $\left(\Phi_R^k \circ \phi_R\right)\left(x_{R,n}^{**}\right) > 0$ for sufficiently large n and $\mu \in [\mu_n^+, \mu_n^-]$, since $\left(\Phi_R^k \circ \phi_R\right)\left(x_{R,n}^{**}\right)$ is linear in μ and positive at $\mu = \mu_n^+$ and $\mu = \mu_n^-$ for large n. Furthermore, it follows from Eq. (87) that $\left(\phi_R \circ \Phi_R^{n-1} \circ \phi_R\right)\left(x_{R,n}^{**}\right) \leq 0$ for sufficiently large n if and only if $\mu \leq \mu_n^-$, since equality holds when $\mu = \mu_n^-$ and the slope of $\left(\phi_R \circ \Phi_R^{n-1} \circ \phi_R\right)\left(x_{R,n}^{**}\right)$ with respect to μ is positive for large n. Finally, for $0 \leq k \leq n-2$, it follows from Eq. (70) that $\left(\phi_R \circ \Phi_R^k \circ \phi_R\right)\left(x_{R,n}^{**}\right) < 0$ for sufficiently large n and $\mu \in [\mu_n^+, \mu_n^-]$, since $\left(\phi_R \circ \Phi_R^k \circ \phi_R\right)\left(x_{R,n}^{**}\right)$ is linear in μ and negative at $\mu = \mu_n^+$ and $\mu = \mu_n^-$ for large n. □

It is again straightforward to show that $\mu_{n+1}^- < \mu_n^+$, i.e., that the intervals of existence of each such periodic orbit are mutually disjoint. From Eqs. (92-93), it follows that $\mu_n^-, \mu_n^+ \downarrow 0$ as $n \to \infty$. Substitution now yields the limiting scaling relationships

$$\lim_{n\to\infty} \frac{\mu_{n+1}^+}{\mu_n^+} = \lim_{n\to\infty} \frac{\mu_{n+2}^+ - \mu_{n+1}^+}{\mu_{n+1}^+ - \mu_n^+} = v \tag{94}$$

and

$$\lim_{n\to\infty} \frac{\mu_{n+1}^-}{\mu_n^-} = \lim_{n\to\infty} \frac{\mu_{n+2}^- - \mu_{n+1}^-}{\mu_{n+1}^- - \mu_n^-} = v. \tag{95}$$

The proof of Claim 4 shows that each interval is bounded by two border-collision bifurcations, corresponding either to $x_{R,n}^{**} = 0$ (when $\mu = \mu_n^+$) or $\left(\phi_R \circ \Phi_R^{n-1} \circ \phi_R\right)\left(x_{R,n}^{**}\right) = 0$ (when $\mu = \mu_n^-$). We again observe an infinite sequence of border-collision bifurcations accumulating monotonically from the right on $\mu = 0$. For n bounded below by N, the periodic orbits are found to be locally asymptotically stability on their respective intervals of existence. Moreover, at $\mu = 0$, a border collision of a period-two orbit coexists with an infinite family of trajectories based arbitrarily close to $x = 0$ and whose even iterates approach $x = 0$ arbitrarily closely in forward time.

A two-dimensional map. A two-dimensional piecewise affine map is obtained from the component maps

$$\phi_L : x \mapsto \begin{pmatrix} 3x_1 - x_2 + 1 + 5\mu \\ -x_1 + 3x_2 + \mu \end{pmatrix} \tag{96}$$

and

$$\phi_R : x \mapsto \begin{pmatrix} (x_1 - 1)/8 \\ x_2/8 \end{pmatrix} \tag{97}$$

applied when $x_1 \leq 0$ and $x_1 \geq 0$, respectively. The family $x_L^*(\mu) = \begin{pmatrix} \mu & 0 \end{pmatrix}^T$ consists of asymptotically stable fixed points of the composition $\Phi_L := \phi_R \circ \phi_L$ that belong to period-two orbits of the piecewise affine map for $\mu < 0$. The largest-in-magnitude eigenvalue of the Jacobian of Φ_L equals $1/2$ with the corresponding eigenvector given by $\begin{pmatrix} -1 & 1 \end{pmatrix}^T$.

We may solve explicitly for the critical values of μ that correspond to border-collisions of periodic orbits of the piecewise affine map corresponding to fixed points of the composition $\Phi_L^n \circ \phi_R$ for arbitrary n. Specifically, in the notation introduced in previous sections,

$$\mu_n^+ = \frac{-1 + 2^{n+2} + 2^{2n+2}}{4(2 - 9 * 2^n - 9 * 2^{2n} + 2^{4+3n})} \tag{98}$$

and the corresponding loci on the discontinuity are given by

$$x_2 = \frac{2^n}{-2 + 7 * 2^n + 2^{2n+4}} \tag{99}$$

In particular,

$$\lim_{n\to\infty} \frac{\mu_{n+1}^+}{\mu_n^+} = \frac{1}{2} \tag{100}$$

as predicted by the general theory.

Let $\Gamma = \{(0, y), y \in (-\delta, \delta)\}$. An illustration of the general argument for the existence of border-collisions of periodic orbits corresponding to fixed points of $\Phi_L^n \circ \phi_R$ is given by the image $\left(\Phi_L \circ \phi_R\right)(\Gamma) =$

$$\left\{ \left(\frac{-3 - y + 40\mu}{64}, \frac{1 + 3y + 8\mu}{64} \right), y \in (-\delta, \delta) \right\}. \tag{101}$$

as shown in Fig. 11.

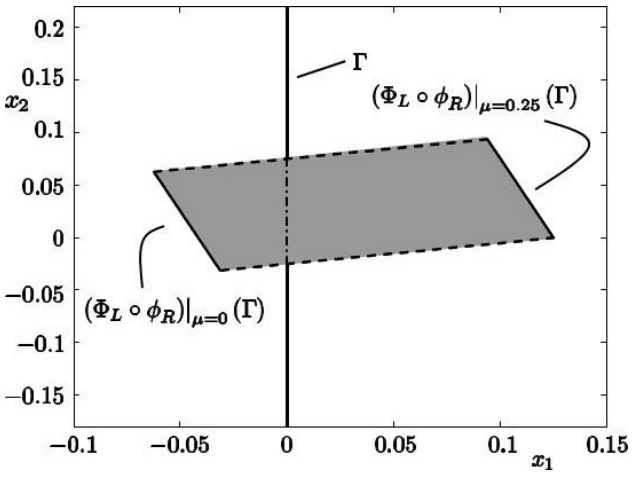

Figure 11: As μ varies between 0 and 0.25, the image $\left(\Phi_L \circ \phi_R\right)(\Gamma)$ of the line segment $\Gamma = \{(0, y), y \in (-1, 1)\}$ sweeps a quadrilateral that intersects the interior of Γ. The induced map from Γ to its interior is a contraction with a unique fixed point at $y = 1/38$.

When $\mu = 0$, all points on the image segment lie in the left half-plane and converge to the origin without crossing into the right half-plane, provided that $\delta < 1$. As μ increases from 0 to 0.25, the image segment sweeps a quadrilateral bounded by the lines $(-3/64, 1/64) + \eta(-1/64, 3/64)$ and $(7/64, 3/64) +$

$\eta(-1/64, 3/64)$, for $\eta \in (-1, 1)$, and $(-1/16, 1/16) + \eta(5/8, 1/8)$ and $(-1/32, -1/32) + \eta(5/8, 1/8)$ for $\eta \in (0, 0.25)$. The map from Γ to the intersection of the quadrilateral with Γ is then given by

$$y \mapsto \frac{1 + 2y}{40} \tag{102}$$

with a unique fixed point at $y = 1/38$, identical to the value obtained from Eq. (99) for $n = 1$.

More detailed analysis of general two-dimensional affine maps is presented in [31].

4.2. Piecewise nonlinear map with gap

We illustrate the existence of border-collision bifurcation cascades in the vicinity of a suitably constrained saddle-node bifurcation of a period-two orbit, as obtained in Sec. 3.2, by restricting attention to the special case of the one-dimensional, piecewise nonlinear map with a gap given by

$$\phi_L(x) := \frac{11}{10} + x \tag{103}$$

and

$$\phi_R(x) := \begin{cases} -\frac{7}{20} + \mu & \text{when } x \le \frac{1}{2} \\ x + (x-1)^2 - \frac{11}{10} + \mu & \text{when } x > \frac{1}{2} \end{cases} \tag{104}$$

Here, $x = -\frac{1}{10}$ and $x = 1$ constitute a nonhyperbolic period-two orbit of the corresponding map ϕ_0 obtained from Eq. (55) when $\mu = 0$. Indeed, for $\mu < 0$, there exist two branches of fixed points of the composition $\phi_R \circ \phi_L : x \mapsto x + (x + 1/10)^2 + \mu$: a sink at

$$x = -\frac{1}{10} - \sqrt{-\mu} \tag{105}$$

and a source at

$$x = -\frac{1}{10} + \sqrt{-\mu}. \tag{106}$$

It is straightforward to numerically determine values of μ for which $x = 0$ is a fixed point of the map $(\phi_R \circ \phi_L)^n \circ \phi_R$ (i.e., μ_n^+) and of the map $(\phi_R \circ \phi_L)^{n-1} \circ \phi_R \circ \phi_R \circ \phi_L$ (i.e., μ_n^-) for different values of the integer n. Indeed, it follows from the form of $\phi_R \circ \phi_L$ that such values must exist for all n and must belong to a decreasing sequence[4] that accumulates on 0. As an example, Fig. 12 graphs the differences

$$d_n := \frac{1}{\sqrt{\mu_{n+1}^+}} - \frac{1}{\sqrt{\mu_n^+}} \tag{107}$$

against n. The convergence toward a nonzero number is again evidence of the scaling relationship $\mu_n^+ \sim n^{-2}$ for large n. Fig. 13 shows an example periodic orbit with $n = 40$ obtained for $\mu = 0.0034$.

[4]It is straightforward to show that, for this example, $\mu_n^- = \mu_{n-1}^+$ for $n \ge 2$.

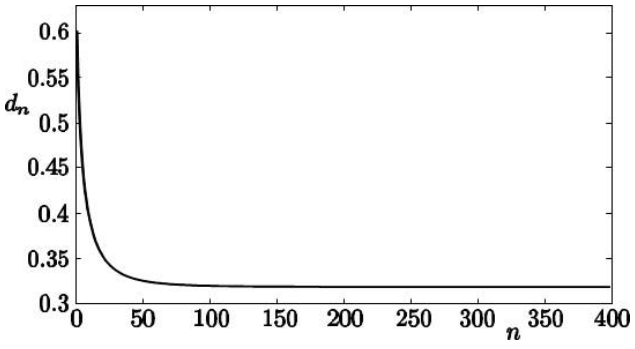

Figure 12: A piecewise linear interpolant through the differences d_n of the reciprocal square roots of the sequence μ_n^+ of border-collision bifurcation values for the map given by Eqs. (103-104) near the saddle-node bifurcation at $\mu = 0$. For large n, the numeric analysis yields $\mu_n^+ \approx 10/(n + 15)^2$.

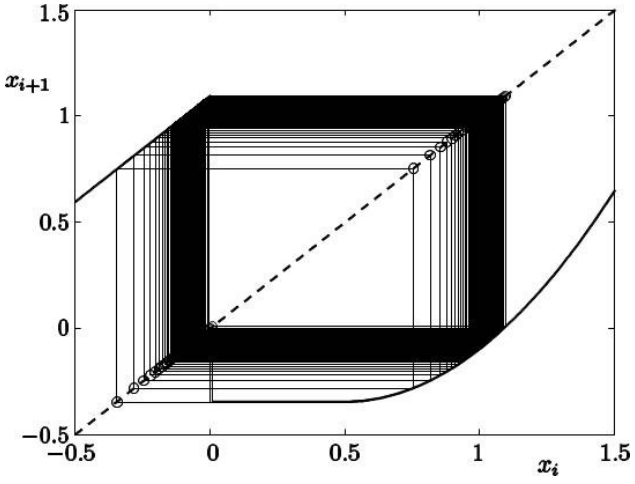

Figure 13: A cobweb representation of a periodic orbit of the map given by Eqs. (103-104) for $\mu = 0.0034$ corresponding to a fixed point of the composition $(\phi_R \circ \phi_L)^n \circ \phi_R$ with $n = 40$. For small μ, the number of iterates near the ghost of the nonhyperbolic period-two orbit grows as $1/\sqrt{\mu}$ [13, 20].

4.3. A forced oscillator

Finally, we note that it is not difficult to construct continuous-time dynamical systems that exhibit the bifurcation cascades considered here. A particularly simple example is the autonomous linear oscillator whose continuous-time dynamics are given by the differential equations

$$\ddot{x} + c\dot{x} + kx = r\cos\theta,\ \dot{r} = \alpha, \dot{\theta} = \beta, \tag{108}$$

and where the time history of r is further coupled to that of x by means of the imposition of the state reset $r \mapsto \rho r$ when x increases through a critical value $\bar{x}$. A numerical example of a near-grazing two-cycle orbit is obtained with $k = 0.3$, $c = 2$, $\alpha = 0.2$, $\beta = 1.3$, $\rho = 0.5$, and $\bar{x} = 1.2$. In the nearby bifurcation cascade obtained under variations in $\bar{x}$, the branch of periodic orbits corresponding to

$n = 1$ contains $\bar{x} = 1.11$ and the branch of periodic orbits corresponding to $n = 2$ contains $\bar{x} = 1.16$. Numerical continuation may again be deployed to locate the solution manifolds and the critical parameter values $\bar{x}_n^+$ and $\bar{x}_n^-$.

5. Concluding discussion

The numerical results in Secs. 2.3 and 2.4 establish within numerical accuracy that the sufficient conditions in Secs. 3.1 and 3.2 (for the existence of period-adding bifurcation cascades) are satisfied by the implicitly defined maps ϕ_{long} and ϕ_{short} at the critical parameter values $k'_{2,\text{grazing}}$ and $k'_{2,fold}$, respectively. That the bifurcation cascades observed in the numerical models are indeed implied by these conditions is further supported by the perfect agreement between the scaling relationships associated with consecutive bifurcation values predicted by the theoretical analysis and those found numerically. Similarly, the relationship between grazing bifurcations in the discretized continuous-time models and border-collisions bifurcations in the piecewise-defined maps establishes with great certainty the phenomenology and the theoretical explanation.

The results of the analysis in Secs. 3.1 and 3.2 apply without modification to the case where the maps ϕ_{short} and ϕ_{long} are defined not by the discretized boundary-value problem (as in Sec. 2.2), but by the continuous-time boundary-value problem obtained from the original system of differential equations modeling the cell cycle. In either case, ϕ_{short} and ϕ_{long} are only implicitly defined by a set of governing equations, finite in the case of the discretized boundary-value problem and infinite in the case of the system of ordinary differential equations with a suitable end-point condition. The theoretical treatment is clearly impervious to the origin of the component maps.

In particular, it follows that the bifurcation cascade observed for the discretized boundary-value problem is as close an approximation to that expected in the infinite-dimensional problem as the approximate piecewise-polynomial functions are to the time histories of the state variables in the original hybrid dynamical system. We chose to emphasize the discretized equations in the treatment in Sec. 2.2 in order to establish a systematic approach to generating numerical results across the entire bifurcation cascade, without reliance on black-box shooting methods (that hide the discretization behind layers of error estimation and step variability). A further benefit to the collocation approach employed in the discretization in Sec. 2.2 over a shooting-based method is the rapid evaluation of the boundary-value problem residuals and the corresponding Jacobians.

Although the discussion in Sec. 3 is restricted to the case of bifurcation cascades organized by period-two orbits, it is straightforward to extend the results to the case of periodic orbits with more complicated orbital signatures. Recall, in particular, the assumed existence of an integer N beyond which every second iterate of the forward trajectory based at $\phi_R(0,0)$ is obtained by successive application of Φ_L. As the subsequent analysis depended only on properties of Φ_L for $(x,\mu) \approx (0,0)$, the conclusions apply immediately to alternative definitions of Φ_L appropriate for different trajectory signatures. A relevant numerical example is obtained by slightly decreasing r in the nine-dimensional cell cycle model, yielding a period-adding cascade, through a sequence of nonconsecutive odd periods, triggered by the grazing of an orbit of period four, rather than two. Another immediate application is to the periodic orbits found at the Type I grazing bifurcations at the distal end of the various intervals of existence in a period-adding bifurcation cascade, provided that these attract the forward iterates of $\phi_R(0,0)$.

Similarly, recall the description of the forward-time dynamics of the cell cycle model based at initial conditions near the fixed point (u^*, m^*) in terms of the application of ϕ_{short} followed by an alternating sequence of ϕ_{long} and ϕ_{short} accumulating on the fixed point. As is evidenced by the theoretical treatment, the exact signature of this transient prior to the return to $\Omega_L \cap B_r(0)$ is of no significance to the claimed existence of a bifurcation cascade. It is thus quite possible to imagine that the application of ϕ_μ to $\Omega_R \cap B_r(0)$ involves a return map of a distinctly different form than that applied near $\phi_L(0,0)$ (see, e.g., Eqn. (104)).

For sufficiently high period (i.e., large n), the analysis in Sec. 3 establishes the period-adding bifurcation-cascade phenomenology as essentially governed by the local dynamics along the one-dimensional slow-(or center-)stable manifold of the fixed point of Φ_L on the discontinuity. No claim may be made for the existence of a single one-dimensional map that approximates the behavior for periodic orbits in the bifurcation cascade further away from the accumulation point. As an example, for larger values of r, it is possible to obtain periodic orbits that exhibit multiple oscillations in the value of u_1 above the critical threshold $\bar{u}_1$ prior to the triggering of cell division. In this case, for low values of n, one cannot exclude the possibility of additional grazing bifurcations, leading to a return map with multiple discontinuities.

It is appropriate to reflect on the biological significance of the bifurcation scenarios observed in the numerical models. Notably, whereas the literature on the design of dynamic models of the cell cycle are particularly concerned with the regulation and feedback cycles responsible for achieving single-cycle periodicity, the numerical analysis as well as explorations not shown here demonstrate a rich dynamic repertoire of these models (cf. Gérard and Goldbeter [21] and the simple autonomous oscillator model in 4.3) for physically reasonable parameters. Indeed, there is an extensive literature in the cell-cycle community showing both experimental and modeling evidence of the regulation of the growth rate of individual cells to ensure a size homeostasis at division (e.g., Marshall *et al.* [22] and Turner *et al.* [23], but see also Hoose *et al.* [24]).

If there is an evolutionary advantage to a robust cell-

cycle duration, then it appears reasonable to assume that the relevant chemical and mechanical activity has been selected for regions of parameter space across which a structurally stable behavior corresponding to single-cycle dynamics is found. In this interpretation, the analysis in this paper gives examples of nontrivial bifurcation scenarios on the boundaries of such operating regions. In fact, the two cascade phenomena observed here appear robust enough to be observed over a range of different values of the 39 parameters in the full model, or the 16 parameters in the simplified model. The phenomenon is also quite robust under alterations in the division rule in Eq. (13) to fractions other than 1/2.

Although we have confined our theoretical attention in this paper to codimension-one bifurcations, we invite further study of the codimension-two scenario obtained with a border collision of a nonhyperbolic periodic orbit with a single eigenvalue at 1 and all other eigenvalues within the unit circle. The work of Avrutin, Gardini, and collaborators [25, 26, 27, 28] on codimension-two bifurcations that serve as organizing centers for piecewise-defined maps as well as on nested period-adding structures should also apply to the present treatment. There is also value in elucidating the relationship between the "homoclinic" behavior associated with the fixed point on the discontinuity and the notion of critical homoclinic orbits (see Gardini *et al.* [29]). Of interest are also Farey tree sequences in gaps (where such exist) between successive intervals of periodic orbits in the bifurcation cascade (cf. Yamaguchi and Ohtagaki [30]). Finally, we are excited by the possibility of finding additional bifurcation cascades induced by a global saddle-node bifurcation.

References

[1] M. di Bernardo, A. R. Chamneys, C. J. Budd, P. Kowalczyk, Piecewise-Smooth Dynamical Systems, Springer London, 2008.

[2] B. Li, B. Shao, C. Yu, Q. Ouyang, H. Wang, A mathematical model for cell size control in fission yeast, Journal of Theoretical Biology 264 (2010) 771–781.

[3] B. Pfeuty, K. Kaneko, Minimal requirements for robust cell size control in eukaryotic cells, Physical Biology 4 (2007) 194–204.

[4] J. J. Tyson, B. Novák, Cell cycle controls, in: C. P. Fall, E. S. Marland, J. M. Wagner, J. J. Tyson (Eds.), Computational Cell Biology, Springer Science+Business Media, Inc., 2010.

[5] Z. Qu, W. R. MacLellan, J. N. Weiss, Dynamics of the cell cycle: Checkpoints, sizers, and timers, Biophysical Journal 85 (2003) 3600–3611.

[6] V. Noel, S. Vakulenko, O. Radulescu, Algorithm for identification of piecewise smooth hybrid systems: Application to eukaryotic cell cycle regulation, Lecture Notes in Computer Science (including subseries Lecture Notes in Artificial Intelligence and Lecture Notes in Bioinformatics) 6833 LNBI (2011) 225–236.

[7] R. Alfieri, E. Bartocci, E. Merelli, L. Milanesi, Modeling the cell cycle: From deterministic models to hybrid systems, BioSystems 105 (2011) 34–40.

[8] S. J. Hogan, L. Higham, T. C. L. Griffin, Dynamics of a piecewise linear map with a gap, Proceedings of the Royal Society A: Mathematical, Physical and Engineering Sciences 463 (2007) 49–65.

[9] P. Dutta, B. Routroy, S. Banerjee, S. Alam, On the existence of low-period orbits in n-dimensional piecewise linear discontinuous maps, Nonlinear Dynamics 53 (2008) 369–380.

[10] B. Rajpathak, H. Pillai, S. Bandyopadhyay, Analysis of stable periodic orbits in the one dimensional linear piecewise-smooth discontinuous map, Chaos 22 (2012) 033126.

[11] P. Glendinning, The anharmonic route to chaos: Kneading theory, Nonlinearity 6 (1993) 349–367.

[12] J. P. Keener, Chaotic behavior in piecewise continuous difference-equations, Transactions of the American Mathematical Society 261 (1980) 589–604.

[13] J. Dias De Deus, R. Dilo, A. Noronha Da Costa, Scaling behaviour of windows and intermittency in one-dimensional maps, Physics Letters A 124 (1987) 433–436.

[14] E. Mosekilde, B. Lading, S. Yanchuk, Y. Maistrenko, Bifurcation structure of a model of bursting pancreatic cells, BioSystems 63 (2001) 3–13.

[15] C. Budd, P. Piiroinen, Corner bifurcations in non-smoothly forced impact oscillators, Physica D: Nonlinear Phenomena 220 (2006) 127–145.

[16] H. Dankowicz, F. Schilder, Recipes for Continuation, SIAM, 2013.

[17] H. Dankowicz, M. Katzenbach, Discontinuity-induced bifurcations in models of mechanical contact, capillary adhesion, and cell division: A common framework, Physica D: Nonlinear Phenomena 241 (2012) 1869–1881.

[18] P. Dutta, S. Banerjee, Period increment cascades in a discontinuous map with square-root singularity, Discrete and Continuous Dynamical Systems - Series B 14 (2010) 961–976.

[19] S. Pring, C. Budd, The dynamics of a simplified pinball machine, IMA Journal of Applied Mathematics (Institute of Mathematics and Its Applications) 76 (2011) 67–84.

[20] J. Duarte, C. Janurio, N. Martins, J. Sardanys, Scaling law in saddle-node bifurcations for one-dimensional maps: A complex variable approach, Nonlinear Dynamics 67 (2012) 541–547.

[21] C. Gérard, A. Goldbeter, From simple to complex patterns of oscillatory behavior in a model for the mammalian cell cycle containing multiple oscillatory circuits, Chaos 20 (2010) 045109.

[22] W. Marshall, K. Young, M. Swaffer, E. Wood, P. Nurse, A. Kimura, J. Frankel, J. Wallingford, V. Walbot, X. Qu, A. Roeder, What determines cell size?, BMC Biology 10 (2012) 101.

[23] J. Turner, J. Ewald, J. Skotheim, Cell size control in yeast, Current Biology 22 (2012) R350–R359.

[24] S. Hoose, J. Rawlings, M. Kelly, C. Leitch, Q. Ababneh, J. Robles, D. Taylor, E. Hoover, B. Hailu, K. McEnery, S. Downing, D. Kaushal, Y. Chen, A. Rife, K. Brahmbhatt, R. Smith, M. Polymenis, A systematic analysis of cell cycle regulators in yeast reveals that most factors act independently of cell size to control initiation of division, PLoS Genetics 8 (2012) e1002590.

[25] V. Avrutin, M. Schanz, S. Banerjee, Codimension-three bifurcations: Explanation of the complex one-, two-, and three-dimensional bifurcation structures in nonsmooth maps, Physical Review E - Statistical, Nonlinear, and Soft Matter Physics 75 (2007) 066205.

[26] V. Avrutin, A. Granados, M. Schanz, Sufficient conditions for a period incrementing big bang bifurcation in one-dimensional maps, Nonlinearity 24 (2011) 2575–2598.

[27] V. Avrutin, M. Schanz, L. Gardini, Calculation of bifurcation curves by map replacement, International Journal of Bifurcation and Chaos 20 (2010) 3105–3135.

[28] L. Gardini, F. Tramontana, V. Avrutin, M. Schanz, Border-collision bifurcations in 1d piecewise-linear maps and leonov's approach, International Journal of Bifurcation and Chaos 20 (2010) 3085–3104.

[29] L. Gardini, I. Sushko, V. Avrutin, M. Schanz, Critical homoclinic orbits lead to snap-back repellers, Chaos, Solitons and Fractals 44 (2011) 433–449.

[30] T. Yamaguchi, H. Ohtagaki, The order of appearance of oscillation modes of a piecewise linear map, Journal of the Physical Society of Japan 65 (1996) 3500–3512.

[31] B. Rakshit, M. Apratim, S. Banerjee, Bifurcation phenomena in two-dimensional piecewise smooth discontinuous maps, Chaos 20 (2010) 033101.